Integration of bifacial photovoltaics in agrivoltaic systems

A synergistic design approach

Katsikogiannis, Odysseas Alexandros ; Ziar, Hesan; Isabella, Olindo

DOI
10.1016/j.apenergy.2021.118475

Publication date
2022

Document Version
Final published version

Published in
Applied Energy

Applied Energy 309 (2022) 118475

Contents lists available at ScienceDirect

Applied Energy

journal homepage: www.elsevier.com/locate/apenergy

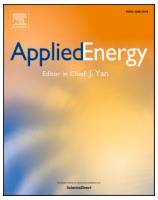

Integration of bifacial photovoltaics in agrivoltaic systems: A synergistic design approach

Odysseas Alexandros Katsikogiannis, Hesan Ziar *, Olindo Isabella

Photovoltaic Materials and Devices Group, Electrical Sustainable Energy Department, Delft University of Technology, Delft, the Netherlands

HIGHLIGHTS

- A multi-scale sensitivity analysis was performed including modifications from module to string to array.
- Various topologies of fixed bifacial agrivoltaic arrays were simulated.
- Design trade-offs and potential synergistic effects were examined.
- The *E-W wings* agrivoltaic array layout was proposed with an extended front glass cover.
- By adopting a translucent cover, blueberries photosynthesized effectively under shade.

ARTICLE INFO

Keywords:
Agrivoltaics
Agrophotovoltaic design
Bifacial solar photovoltaic optimization
Radiance/Daysim simulation
Multi-scale sensitivity analysis
Land equivalent ratio

ABSTRACT

To safeguard future renewable energy and food supply the use of agrophotovoltaic (APV) systems was investigated, which enable simultaneous production under the same piece of land. As conventional photovoltaic (PV) array topologies lead to unfavourable conditions for crop growth, the application of APV is limited to areas with high solar insolation. By optimizing the APV array's design, compatibility with various climates and crop species can be attained. Therefore, the aim of this research was to establish a multi-scale modelling approach and determine the optimal topology for a medium-to-large-scale fixed bifacial APV array. Three main topologies were analyzed under the climate of Boston, USA: S-N facing, E-W wings, and E-W vertical. For each topology, respectively, specific yield was amplified by 39%, 18%, and 13% in comparison to a conventional monofacial ground mounted PV array. E-W vertical is more appropriate for permanent crop species, while S-N facing necessitates the cultivation of shade tolerant crops during summer as electricity generation is prioritized. The E-W wings APV topology combines the best of both; light is distributed homogeneously, and crops are effectively shaded at noon. To promote the growth rate of blueberries under shade, customized bifacial modules were integrated (arranged as the E-W wings). Land productivity enhanced by 50%, whereas electrical AC yield reduced by 33% relative to the conventional and separate production. Through this holistic approach, it is possible to achieve a comprehensive understanding of the limitations and potential synergies associated with the dual use of land; ultimately, encouraging the transition of the agricultural sector into sustainability.

1. Introduction

The continuous development of solar photovoltaic (PV) technologies coupled with rapid cost reductions and advances in conversion efficiency have resulted in a remarkable reduction of the levelized cost of electricity (LCOE) of ground mounted PV (GMPV) [1]. Therefore, their economic competitiveness is promoted, which is essential as the global energy consumption is projected to rise by 50% from 2018 to 2050 [2]. To mitigate any further intensification of global climate change, this energy should be supplied by renewable sources, such as PV; however, due to the relatively low PV module efficiency substantial land coverage would be required to meet this demand. This could be partially alleviated through aggressive installation of building integrated PV (BIPV); nonetheless, the rising demand for GMPV will inevitably lead to the establishment of these systems on agricultural land [3]. One promising solution is the application of agrophotovoltaic (APV) [4] or agrivoltaic [5] systems that permit the simultaneous cultivation of crops and production of renewable electricity; consequently, diminishing the land-use conflict. In this work both terms were used interchangeably as they refer to stilt mounted PV systems elevated above cropland.

* Corresponding author.

https://doi.org/10.1016/j.apenergy.2021.118475
Received 12 July 2021; Received in revised form 1 November 2021; Accepted 25 December 2021
Available online 12 January 2022

To satisfy crop specific needs, some innovative technologies have emerged such as concentrator PV (CPV) [6], and semi-transparent PV achieved either spectrally [7], or regionally [8]. The main drawback of micro CPV is mass production [9] and subsequently cost, while organic PV (OPV) are still premature for large-scale installations due to their reduced efficiency [10] and degradation [11]. For the latter additional performance testing should be achieved to ensure compatibility with in-field conditions and various crop [12–14]. Contrary, by adopting c-Si bifacial cells, whose market share is expected to be at least 35% by 2030 [15], APV could also benefit from the evolving learning curve. In addition, as the maximization of specific electrical yield is of increasing importance for solar installations, the integration of bifacial PV and their potential synergistic behavior with crop cultivation becomes intriguing.

While the concept of APV was conceived in 1981 [4], only a limited amount of modelling frameworks is available, and up to the authors' knowledge these are restricted to the use of conventional PV module and cell arrangements. Such topologies can lead to intense and non-homogeneous shading, which can be detrimental to crop productivity, especially in regions with limited solar insolation. By examining several PV topologies and performing customizations in the design of modules, the needs of crops can be met more appropriately.

The aim of this study is to present a multi-scale modelling framework for deriving the optimal topology for a medium-to-large-scale and static bifacial agrivoltaic array. For all the simulations performed, we used Boston, USA (42.37N, 71.01W) as the study's location. Although in southern climates the potential of such systems would be higher, an agricultural solar tariff unit has been in effect in MA, USA since April 2018 [16]; thus, promoting their deployment.

At first, an extensive literature review on the various environmental and genetic factors that influence the growth rate of plants was achieved. In addition, the impact of diffuse light and shade casted by the PV array on crop productivity were also explored. This review was concluded with studies relevant to bifacial PV optimization and selection of the most appropriate optical modelling technique when integrated in APV systems. The development of the Radiance model followed, along with the AC electrical and crop yield models. A multi-scale sensitivity analysis was carried out, which included modifications ranging from module-to-string-to-array, to identify parameters that have a dominant impact on APV performance. In specific, three main PV topologies were investigated, and their performance was evaluated. Lastly, the potential of a customised bifacial PV module for APV applications was examined.

2. Literature review

2.1. Plant productivity and growth

The rate of photosynthesis is influenced by a plethora of environmental factors – light intensity and homogeneity, available carbon dioxide, ground and ambient temperature as well as humidity – that are interrelated. To successfully photosynthesize, plants require CO_2 which they obtain through their pores. These stomata are hydraulically operated valves that control the size of the opening according to external climatic conditions and the plant's water availability [17]. When there is enough water, they become swollen and allow the uptake of CO_2. However, under conditions of water stress, either due to high irradiance and temperature, or low humidity, they become flaccid and obstruct the process of photosynthesis (hydropassive closure) [18].

Similar to PV cells, leaf absorptance depends on the spectral distribution of the incident light. The portion that is useful for photosynthesis corresponds to the visible spectrum and it is termed as photosynthetically active radiation (PAR) (μmol m^{-2} s^{-1}). The minimum light intensity required to balance the opposing processes of respiration and photosynthesis is known as the light compensation point (LCP), while at a sufficiently high photon flux the rate of growth saturates, denoted by the light saturation point (LSP) (Fig. 1). Essentially, incident irradiance

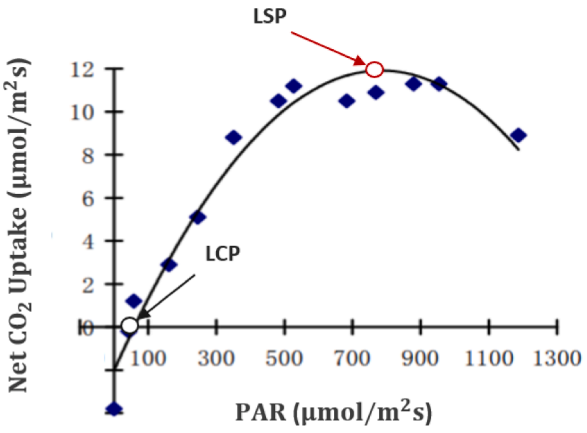

Fig. 1. Photosynthesis light response curve of highbush blueberry leaf (*Vaccinium corymbosum*) under open-field conditions [18].

that exceeds saturation cannot be utilized, rather it is converted into heat, thus reducing productivity. This is directly relevant to hydropassive closure which occurs during midday, leading to a transient reduction in the plant's photosynthetic capability [19]. Subsequent opening of the stomata occurs when the water shortage has been fulfilled.

In addition to environmental conditions, there are also crop specific genetic factors such as plant architecture, and carbon assimilation pathway that greatly impact the process of photosynthesis [20]. Based on the latter, crops can be divided into C3 and C4 species. Naturally, as C3 crops tend to saturate at a significantly lower PAR [21], they are preferable for cultivation under an agrivoltaic array. Furthermore, although shade tolerance is a trait that can be inherited [22–28], C3 species outperform C4 when grown under low light conditions [29–30]. In general, shade-grown leaves experienced a reduction in number and thickness, while their surface area increased [23,31–38]. By occupying a larger area leaves can intercept light more efficiently. Furthermore, under shade, a large vascular network is unnecessary, thus such tissue is substituted by photosynthetic cells. This acclimation to low light conditions was found to be more intrinsic for C3 species [39]; consequently, enhancing their compatibility with APV.

2.2. Diffuse light

Depending on crop architecture, a more uniform horizontal and vertical distribution of light could improve light interception throughout the canopy and subsequently enhance growth. Crop canopies that are short and compact result in substantial self-shading [40]; which could be compensated through an increase in diffuse light. Contrary, canopies with a low leaf area index (LAI), are associated with minimal self-shading and thus do not necessitate a diffuse cover [41]. For instance, the photosynthetic behaviour of cucumbers was enhanced when light penetration throughout the canopy was increased [42]. A similar boost in productivity was observed during cloudy skies, or under forests [43–46]. Therefore, diffuse light can penetrate deeper into the lower leaves of the canopy [47–48].

To amplify the fraction of diffuse light, covering materials like those in greenhouses [49–50] could be examined. The integration of a light diffusion film increased plant production by 5%, thus ensuring profitability [51]. This was verified for various plants; cucumbers with 8% increase, roses with 10%, and tomatoes with 8–11% [52–54]. Light interception amplified on clear days, especially in the middle layers of the canopy [55], thus complementing photosynthetic performance [47,52,55]. This could also be explained by the decreased crop temperature (around half a degree) at the top of the canopy [52,54].

Overall, a diffuse cover enhances the spatial distribution of light, and depending on the plant's architecture, species, and local climatic

conditions the increase in photosynthetic rate and thus productivity can be substantial. Therefore, such a cover could be greatly beneficial in APV systems.

2.3. Influence of the PV array

With the integration of the PV array various microclimatic alterations are anticipated – depending on topology – that can directly influence the photosynthetic rate of the canopy and ultimately its biomass production. Researchers in [56] concluded that only a few adaptations are required to switch from open cropping to APV, instead one should emphasize on mitigating light reduction and selecting crops that could adapt under such conditions.

Experimental results indicated that mean daily air temperature did not vary significantly relative to full sun (FS) conditions [56]. On the other hand, soil temperature reduced under shade casted by the PV array. This reduction in temperature can lead to a decrease in soil evaporation; ultimately, increasing crop yield as was observed for maize in [57] for non-irrigated conditions. In addition, crops were cooler throughout the day, especially around solar noon, while at night the opposite occurred [56,58]. This, in combination with the reduced evapotranspiration rate promoted improved conditions for photosynthesis and growth for some species [56,59].

Naturally, these microclimatic changes will depend on local climatic conditions and PV topology, while the associated influence on crop yield will differ across the various crop species [60]. It is beyond the scope of this paper to exhaust all the potential factors. Nonetheless, based on the aforementioned findings a reasonable estimate of crop yield reduction can be formulated, which will be further discussed under Section 3.4 Performance indicators.

2.4. Bifacial PV optimization

Through the utilization of bifacial solar cells significant reductions in

Table 1
Literature review of various studies related to optimization of bifacial PV [61,64–85].

Elevation (h_M)	Tilt angle (θ_M)	Row spacing (RS)
Single module *a = 0.50, summer day Cairo, EG (30° N)* Standard deviation of rear irradiance can be reduced to 3-4% for an elevation of 1 m [64].	*Various system sizes* *Various albedos & locations* Optimum tilt was latitude inclined like in monofacial [72], or slightly higher [68]. In fact, for the same orientation bifacial outperform monofacial [61, 73]. Increasing trend in optimal tilt for ground mounted modules [64, 67-68], and/or higher albedo [67], and/or northern latitudes [64, 67-68]. Sensitivity of optimum tilt to elevation decreased with increasing elevation [64, 67], and became negligible for clearances > 1 m [68].	*Array (3x11) – θ_M = 25°, h_M = 1.5 m* *Various albedos, El Gouna, EG (27° N)* Logarithmic trend between RS and bifacial gain, while with increased albedo the sensitivity to RS was higher. The gain of modules at the edges of the array was further enhanced. Specifically, for an albedo of 0.5 and a RS of 2.5 m, bifacial gain varied from 27.7 to 31.4% [75]
Single module – tilt 37° *α = 0.21, G_f = 1000 Wm^{-2}, DHI = 100 Wm^{-2}, α_S = 42°* Spatial non-uniformity of rear irradiance was 5% for an elevation of ~1 m [65].	*Array (5x5)* *Various albedos & locations* Optimum tilt was higher for an array and was more sensitive to albedo [68].	*Array (20x20) – various topologies* *Tel-Aviv, IL (32° N)* Increasing the RS from 2.9 to 3.9 m led to an annual increase of incident irradiance by 1% for S-N topologies, while for E-W vertical it resulted in 7.9% [74]. Nonetheless, S-N topologies produced 32% more energy than the latter [74].
Single module – various tilts *Various albedos and locations* Saturation of rear irradiance [65] and annual energy yield [66-67] gain at an elevation of ~2 m [65]. Sensitivity to elevation increased for locations closer to the equator [66-67], and for higher albedo [64, 66-67].	**Orientation: tilt (θ_M) & azimuth (A_M)**	*Array – Ground mounted E-W vertical* *a = 0.5, various latitudes & clearness indices* For regions where irradiance was dictated by DNI a low p/h ratio would be optimum, while the opposite was true when DHI was dominant. Similarly, for latitudes below 30 the ideal p/h was ~0.8, while for northern sites higher values are optimal [76]. Given a RS of 2 m an E-W vertical bifacial array produced 10-20% more annual energy yield in comparison to an optimally inclined monofacial array virtually throughout the globe [76].
Single & string of modules – various tilts *Various albedos & locations* Logarithmic trend between elevation and rear irradiance [65], bifacial gain [68], as well as energy yield [64, 66-68].	*Single module – various topologies* *Tel-Aviv, IL (32° N)* S-N topologies (south facing and optimally inclined) displayed a significantly lower sensitivity to azimuth in comparison to vertically installed [74]. For the latter, E-W facing maximized annual incident irradiance.	
Array (5x5) – various tilts *α = 0.21, clear day in Albuquerque, USA (35° N)* Linear trend between elevation and bifacial gain as well as energy yield of central module [68].	*Single module – E-W vertical* *Various albedos & locations* Can outperform S-N topologies for an albedo of 0.5 and site latitude below 30 degrees [66]. For an elevation > 1 m S-N topology was optimal globally [66].	**Albedo (α)**
Transparency (T_M)		*Crop reflectance* Differences in optical properties amongst species are based on pigments such as chlorophylls and carotenoids [77]. Reflectance of thirty-two plant species [78-79]. For a more detailed spectral distribution: bean, avocado, sorghum, and pigweed [80] potato, alfafa, canola, and oat hay [81] cotton, wheat, and rye [82-84]. Reflectance of apple, orange, nectarine, and pear fruits varied from 60-80% in the infrared [85].
Single module – tilt 37° *α = 0.21, Gf = 1000 Wm-2, DHI = 100 Wm-2, α_S = 42°* For low clearances (< 0.5 m), increasing module transparency by 50% resulted in a gain of rear irradiance by ~10%, while for 1 m the gain was 3.8% [65].		
The operating temperature of bifacial PV is lower than monofacial due to the glass rear cover [69-70]. Further reduction occurred when module transparency was increased due to improved heat dissipation [71].		

PV system LCOE are expected in comparison to their monofacial counterpart [61]. To address bifacial specific benefits a literature review of the main parameters influencing their performance was achieved (Table 1).

Rear side power generation and thus overall energy yield are dependent on the bifaciality factor (*BF*) defined as the ratio of rear side efficiency to front side efficiency under standard test conditions (STC):

$$BF = \left(\eta_{STC,r}/\eta_{STC,f}\right)\cdot 100\% \quad (1)$$

To measure the relative energy yield gain the bifacial gain (*BG*) was used which is defined as the ratio of rear side annual energy yield (kWh/yr) to front side:

$$BG = \left(Y_{e,r}/Y_{e,f}\right)\cdot 100\% \quad (2)$$

For experimental or small demonstration systems BG is expected to vary 15–25%, while for PV farms 5–15% [62]. Besides design criteria, albedo has a significant influence on bifacial gain as well.

The integration of bifacial PV in agrivoltaic applications offers various synergistic effects. As stilt mounted APV systems are significantly elevated from ground level, rear irradiance homogeneity is enhanced, thus omitting one of the main limiting factors in bifacial performance [63]. Coupled with the increase in view factor (VF) from PV to unshaded ground, the magnitude of rear irradiance and subsequently BG also benefit. To allow sufficient light for crop cultivation, APV arrays are deployed at lower densities; consequently, BG is further boosted. As a result, other PV topologies become compelling such as vertically installed and E-W facing (E-W vertical), which could expand the diversity of crops cultivated. Finally, the combination of convective cooling due to high elevation and the microclimate below could reduce the array's operating temperature, enhance its efficiency, and energy yield [59,86]. Moreover, PV integrated in agrivoltaics could benefit from the reduced operating temperature extremes [59], potentially increasing the module's lifetime and solidifying the overall synergistic behaviour.

2.5. Ground albedo

The albedo can vary according to optical and morphological properties of surroundings and based on PV configuration among others [87]. However, for APV systems, ground albedo will also be crop-specific and thus change seasonally as well [88]. Crop architecture is particularly important [89], especially canopy height and LAI, as additional ground shading can occur leading to a reduction of the overall albedo. This would also depend on planting density and the crop's phenological stage.

The fraction of light transmitted through the crop I could be estimated through Beer-Lambert's law [90]:

$$I = I_0 e^{-kx} \quad (3)$$

where I_0 is the irradiation incident on a horizontal plane on the top of the canopy. The light extinction coefficient k accounts for the influence of leaf arrangement and tilt [91], which was estimated to be between 0.7–1.0 and 0.3–0.5 for horizontal and vertical leaves respectively [90]. The variable x describes the cumulative LAI of the canopy along the vertical direction. For most agricultural systems to be productive LAI values usually lie between 3 and 5 [20].

Additional complications arise when considering that in natural stands the lower leaves are oriented closer to horizontal, while in the upper layers they are more erect. To represent a more realistic case of the irradiation incident on the canopy plane $I^{'}$, additional modifications can be performed on Eq. (3) [91]:

$$I^{'} = \frac{I_0 k e^{-kx}}{\left(1-\tau_{leaf}\right)} \quad (4)$$

where τ_{leaf} is the leaf's transmittance. Although omitted in this paper, if parameters k, and x are known then Eq. (4) can be used to estimate the amount of light intercepted by the leaves.

Other surfaces that heavily impact light intensity and distribution throughout the farm are reflective mulches [92–93]. When coupled with decreased PV densities, light demanding crops could be cultivated. Such an alternative is compelling as specific electrical yield (kWh/kWp) of bifacial PV arrays would be enhanced.

2.6. Ray tracing validity

To achieve the objective of this study, the modelling approach utilized should be robust, yet flexible in manipulating the PV topology, while addressing detailed features of the design such as cell spacing [98–100]. Bifacial arrays that are close to ground mounted can be accurately modelled with either approach; VF, or ray tracing (RT) [94]; however, after a certain elevation the VF model heavily underestimates rear-side irradiance [96–97]. Consequently, in this study RT was adopted for the optical modelling of bifacial stilt mounted APV.

An increasing number of studies have explored the use of RT and more specifically Radiance for the derivation of rear-side irradiance, thus justifying its reliability for various system sizes, topologies, and climates (Table 2). Note that both bifacial_radiance (developed by NREL) [103] and Franhofer ISE RT [98] software are based on Radiance [104]. Radiance is a physically based illuminance mapping software, which recursively solves Kajiya's rendering equation [105] using backward RT [104]. The propagation of electromagnetic waves is simulated as rays travelling in straight lines, while interactions are described through refraction and reflection at each boundary (ray optics).

RT is associated with an increased computational burden. To speed up the computation, Radiance based daylighting simulation tool Daysim [106] could be adopted without a significant loss of accuracy [107]. Its performance was compared to measured data and the relative error was found to be less than 2% [108], which was attributed almost equally to both Perez model [109] and Radiance's algorithm. For overcast conditions modelled and measured values coincided [108,110], while for clear skies the error was between 5 and 10%, and for intermittent 10–15% [110]. Overall, considering the disparate collection of PV topologies and the time limitation the combination of Daysim and Radiance was deemed as a more practical alternative.

3. Methodology

The modelling framework and tools utilized are summarized in Fig. 2, which is divided into three stages: geometric, irradiance, and yield modelling. In the first phase, a CAD model of the APV system was generated. Due to the plethora of parameters necessary to define such topologies, Grasshopper [111] – a plug-in of Rhinoceros – was incorporated as it offers precise parametric control. After assigning material properties to each geometry and selecting Radiance parameters, RT was initiated for the surfaces of interest, front and rear PV side, as well as ground. Irradiance modelling was performed with Radiance's RT algorithm in combination with the daylight coefficient approach of Daysim and the Perez All Weather sky model [109]. The intensity and distribution of irradiance could then be visualized. To couple geometric with irradiance modelling, an environmental analysis tool was used, DIVA [112]. The third stage involved the utilization of the simulated irradiance/irradiation values along with the underlying climatic conditions to model crop and AC electrical yield. The latter depends on PV module operating temperature and conversion efficiency along with various DC to AC losses, which will be further elaborated. This procedure was iterated for various PV topologies and based on the land's productivity the most optimal was identified.

Table 2
Studies concerning the use of ray tracing (RT) for irradiance modelling of bifacial PV systems [62,68,94–102].

bifacial_radiance RT, MoBiDiG quasi-3D VF, and PVSyst 2D VF	**EDF RT**
Array (5 rows) – $h_M = 0.15\ m$, $\theta_M = 30°$, $\alpha = 0.5$, one-month accumulated irradiation in Konstanz, GE (48° N) Both RT (non-cumulative) and VF approach can model rear irradiation with an accuracy between +-0.5% to +-2% [94]. Deviation varied with climatic conditions [94] which was also verified by [68, 95].	*Small-scale array – $GCR = 50\%$, $\theta_M = 30°$, $\alpha = 0.30$, three-month period, Paris, FR (49° N)* The error in estimating energy yield was less than 1% [99].
bifacial_radiance RT, MoBiDiG VF, PVsyst VF	**Cell-level VF, Radiance RT, COMSOL RT**
Array (unlimited rows & columns) – $GCR = 33\%$, $h_{hub} = 2.1m$, horizontal single axis tracking (HSAT), $\alpha = 0.28$, four-month simulation period in Coquimbo, CL (30° S) Front irradiation remained almost constant with increasing elevation from ground; however, rear irradiation gained significantly. The simulated BG for each corresponding modelling approach used were 9.3%, 6.8%, and 6.5%, respectively, while the measured value varied from 10.4-12.4% [96].	*Array (2x4) – $h_M = 1m$, $\theta_M = 40°$, $\alpha = 0.20$, solar noon April in Albuquerque, NM ((35° N)* For front irradiance, Radiance resulted in 5% lower values when compared to the other, while for the rear-side, it led to an overestimation [100].
Fraunhofer ISE RT software, PVsyst VF	**Radiance RT**
Hourly to annual data: 1. *String (1x8) – $h_M = 1.5\ m$, $\theta_M = 37°$, $A_M = 217°$, $\alpha = 0.2$, Siheung, KR (34° N)* 2. *Array – $GCR = 40\%$, $h_M = 6.6\ m$, $\theta_M = 20°$, $A_M = 234°$, $\alpha = 0.55$, Heggelbach, DE (48° N)* Mean biased error MBE between simulated and measured values [97]: For front irradiance PVSyst resulted in 4.6% and 4.9%, while F. ISE yielded 6.3%, and 2.9% for system 1 and 2, respectively. Similarly, for rear irradiance PVSyst resulted in -21.5% and -23.2%, while F. ISE yielded -3.9% and -3.5%.	1) *Single module – varying tilt, hourly data* 2) *Single module – varying tilt, reflector, solar noon September* 3) *Array – $h_M = 0.2\ m$, $\theta_M = 15°$, $\alpha = 0.64$, annual data* 4) *Array (4x16) – various tilts, $h_M = 1\ m$, $\alpha = 0.21$, clear day in Albuquerque, NM (35° N)* 1) Simulated irradiance incident on PV deviated more for high tilt angles (~ +10% error for $\theta_M = 90°$) [68] 2) Simulated I-V characteristics displayed a good agreement with experimental under the sun measurements [101]. 3) Simulated & measured BG of 21.1% & 21.9%, respectively [62]. 4) Root mean squared error RMSE of front and rear-side irradiance of central module in each row varied between 4.6-6.8% and 4.3-16.4%, respectively (cumulative RT approach) [68].
Fraunhofer ISE RT, Electricite de France EDF RT	**Fraunhofer ISE RT, Electricite de France EDF RT**
Various timescales & climates ▪ *Single module – varying tilt, $\alpha = 0.25$* ▪ *Small-scale array – $\theta_M = 30°$, $\alpha = 0.30$* ▪ *Small-scale array – E-W HSAT, $\alpha = 0.30$* ▪ *Large-scale array – $\theta_M = 12°$, $\alpha = 0.32$* The average total error in deriving POA irradiance and energy yield was between 3-7% [98] for a variety of climates, array topologies and sizes, as well as tracking systems.	▪ *Single module – various tilts, $\alpha = 0.25$, 15th July in Freiburg, GE (48° N)* ▪ *Small-scale array – GCR = 50%, $\theta_M = 30°$, $\alpha = 0.30$, from 27th Jun to 30th Dec in Paris, FR (49° N)* ▪ *Small-scale array – GCR = 35%, E-W HSAT, $\alpha = 0.30$, from 17th Aug to 18th Feb in California, US (37° N)* ▪ *Large-scale array – GCR = 70%, $\theta_M = 12°$, $\alpha = 0.32$, from 1st Aug to 28th Feb in Israel* The average total error in deriving POA irradiance and energy yield was between 3-7% [98]. For single modules RMSE varied from 3-5%, while for small-scale systems it was in the range of 5-7%. Furthermore, the DC yield errors were lesser than those obtained from standard tools used to simulated monofacial PV [102].

3.1. Geometric modelling

The aim of the geometric model was to interrelate all the parameters that establish the APV topology. This was accomplished by conducting a multi-scale (array-string-module) parametrization in 3D (Fig. 3). Starting from the "micro" scale, cell dimensions, number, and spacing, were all parametrically defined. Front, and rear cover as well as aluminium frame were included to define a single module. By varying the inter-column-spacing (ICS) and inter-row-spacing (IRS), or through additional rows per row, numerous arrangements were examined. Finally, the string of modules was converted into an array based on the specified row spacing (RS) and column spacing (CS).

The support structure and its associated shading effect on crops are omitted throughout the analysis, as conventional mounting structures could lead to an underestimation of the actual light intensity on ground. Though the impact cannot be assumed negligible, there is a great deal of an on-going effort to meticulously design such elements to further optimize APV system performance.

3.2. Irradiance modelling

The optical properties of each geometry were either obtained from literature or estimated as listed in Table 3. Note that the seasonal variation of ground albedo is disregarded, as 3D modelling of interactions between light and crops is quite complex.

After the APV topologies were parametrically defined and material properties were assigned to each geometry, the sizing of each sample followed. As it is computationally infeasible to simulate large-scale systems, only a portion was modelled. Nonetheless, to faithfully represent the underlying shading conditions the sample size of the APV array was significantly larger than the farm's as shown in Fig. 4 (a). In fact, as agrivoltaic arrays are highly elevated shadow length is extended; consequently, the adopted sample size was bigger than then one suggested in [96] for modelling of bifacial PV systems. Furthermore, by positioning the farm sample right at the centre of the array the influence of border effects was mitigated, as would be the case for the central region of a large-scale system.

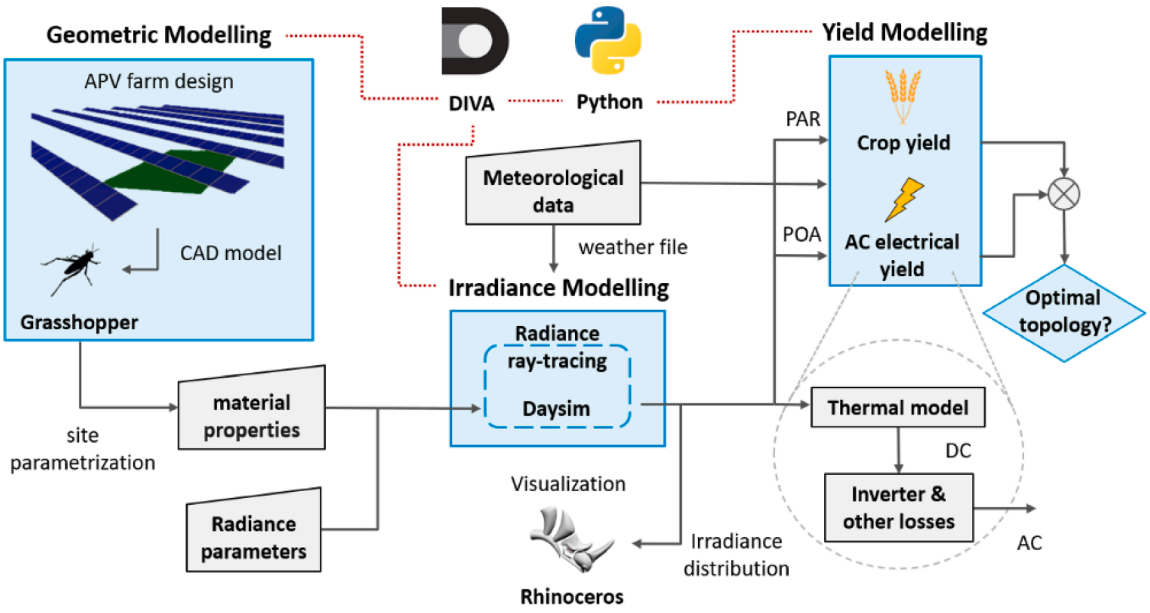

Fig. 2. APV system modelling framework. Rigid lines display the flow of data, while dotted and red lines couple each stage with DIVA through Python. Trapezoids and squares represent inputs and models, respectively. On the bottom right the AC yield model is deconstructed.

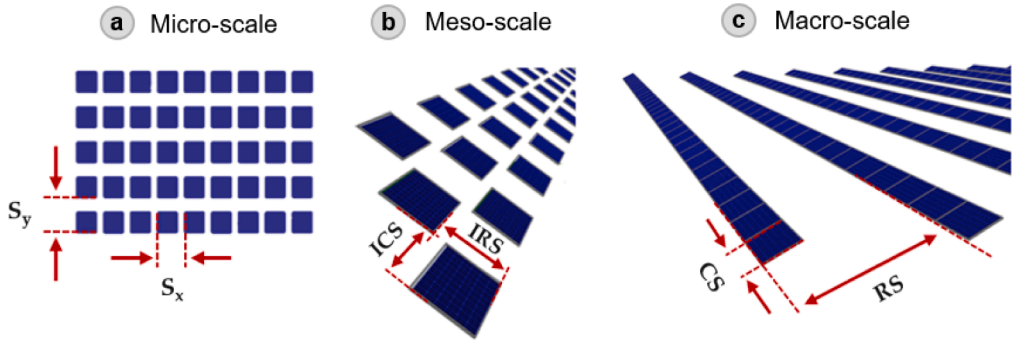

Fig. 3. Multi-scale parametrization of APV topologies: (a) single module, (b) string, (c) array.

Table 3
List of optical properties for each geometry.

Geometry	Optical properties	Radiance material description							
Soil	20% diffuse reflectance [119–121]	plastic	0.25	0.25	0.10	0	0		
PV cell	10% diff. refl. [122–126]	plastic	0.10	0.10	0.10	0	0		
PV module frame	30% diff. & 40% specular refl. [125–126]	metal	0.30	0.30	0.30	0.4	0		
Glass cover	88% normal transmittance [123,127]	glazing	0.88	0.88	0.88				
Translucent cover (SG80)	84% hemispherical transmit., 78% haze factor [50]	trans	1	1	1	0.04	0.05	0.869	0.22

Diffuse reflectance is the fraction of light that is scattered off a surface at various angles, while specular refers to a single outgoing direction.
Normal transmittance signifies the amount of light transmitted for a ray that is perpendicular to the surface of interest, while hemispherical quantifies the overall transmission for various incident angles throughout the hemisphere. The haze factor is defined as the ratio of diffuse to overall transmittance.

Irradiance incident on the solar array was simulated for only a fraction of it, which was defined as the PV modelling sample (Fig. 4 (b)). Since bifacial PV heavily rely on reflected irradiance – depending on topology – the ground was extended and the gain in VF from ground to PV was recorded (Fig. 4 (c, d, e)). The size of ground adopted agreed with [113]; however, it was undersized in comparison to that of [64] to reduce computational burden. Note that for crop yield modelling the surface area covered by the farm sample was used instead.

Table 4 presents a list of Radiance parameters adopted.

3.3. Electrical AC yield

In this section, the procedure of converting the plane of array (POA) irradiation to annual AC electrical yield is elaborated. Most of the associated losses in this conversion are estimated through literature findings, a summary of which is listed in Table 5. Although an in-depth electrical performance model was not formulated, the distinct differences between topologies remained intact and insightful.

A recent experimental study concluded that significant soiling rates of up to 0.35%/day were present on an agrivoltaic array located in Chile [114]. Naturally, this is expected to vary based on region, agricultural activities during certain periods (tillage, harvesting), as well as PV array

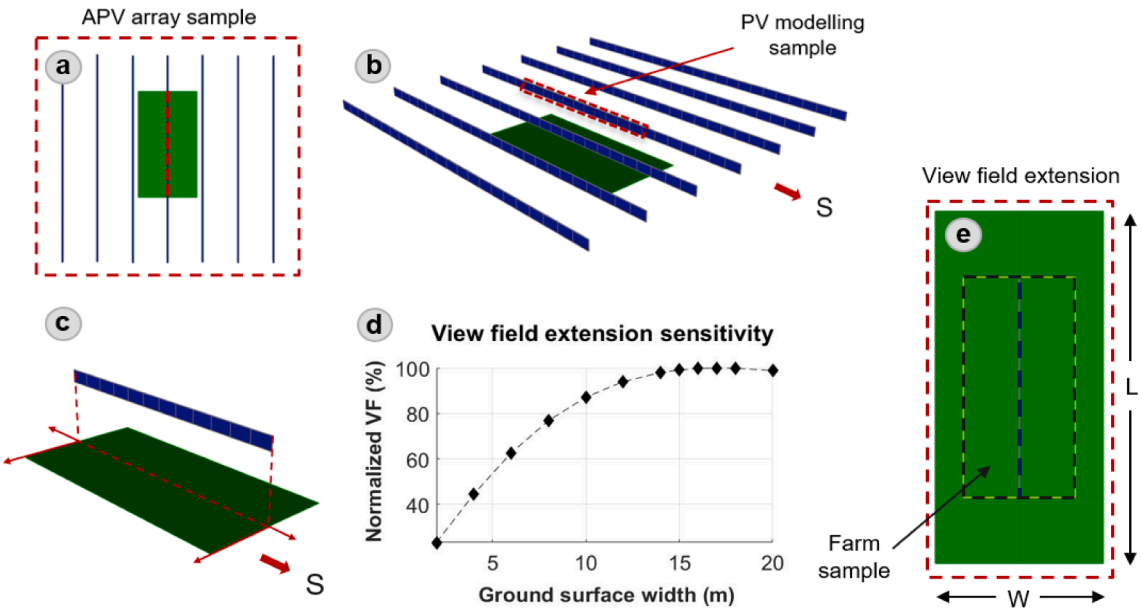

Fig. 4. (a) APV array top view, (b) central string of modules for irradiance modelling, (c) farm sample (10 × 20 m^2), (d) VF gain for E-W vertical PV topologies, (e) total ground patch (15 × 32 m^2).

Table 4
Summary of Radiance parameters.

Ambient bounces (−ab) [1]	Ambient division (−ad)	Ambient sampling (−as)	Ambient accuracy (−aa) [2]	Ambient resolution (−ar)
4	1024	256	0.25	256

[1] −ab 4 for ground, while −ab 5 for front and rear PV side.
[2] −aa 0.1 for the cell spacing sensitivity.

tilt angle and elevation. The power losses due to soiling could be mitigated by integrating PV cleaning with an irrigation system [115]. Nonetheless, to estimate the annual soiling losses the value obtained from [116] for an industrial area in Boston, USA was modified based on module tilt angle according to the trends provided in [117–118].

To relate the plane of array irradiance G_{POA} with the module's electrical performance – short circuit current I_{sc}, open circuit voltage V_{oc}, maximum power point P_{mpp} – and efficiency the following equations were used:

$$I_{sc}(25^{\circ}C, G_{POA}) = I_{sc}(STC)\frac{G_{POA}}{G_{STC}} \tag{5}$$

$$V_{oc}(25^{\circ}C, G_{POA}) = V_{oc}(STC) + N_s\frac{nk_BT}{q}ln\left(\frac{G_{POA}}{G_{STC}}\right)_{|T=25^{\circ}C} \tag{6}$$

$$P_{mpp}(25^{\circ}C, G_{POA}) = FF{\cdot}V_{oc}(25^{o}C, G_{POA}){\cdot}I_{sc}(25^{o}C, G_{POA}) \tag{7}$$

$$\eta(25^{\circ}C, G_{POA}) = \frac{P_{mpp}(25^{\circ}C, G_{POA})}{(G_{POA}{\cdot}A_{m,act})} \tag{8}$$

where N_s is the number of cells in series, n is the ideality factor (assumed as one), and $A_{m,act}$ is the active surface area. These constants along with the module's STC characteristics were derived from the data sheet in [133].

The effect of temperature was accounted for through the SNL model [134], which was claimed to be more accurate than the NOCT [135–137], and others that consider wind-induced convection (e.g. Faiman [138]) under certain conditions. The following equation was used to estimate the module's operating temperature T_m [134]:

$$T_m = T_{amb} + G_{POA}{\cdot}e^{(a+b{\cdot}w)} \tag{9}$$

where the coefficients (a, b) were estimated to be −3.47 and −0.0594 respectively.Then, the influence of operating temperature was coupled to determine the actual P_{mpp} [139], and module efficiency:

$$P_{mpp}(T_m, G_{POA}) = P_{mpp}(25^{\circ}C, G_{POA})[1 + \kappa_P(T_M - 25^{\circ}C)] \tag{10}$$

$$\eta(T_m, G_{POA}) = \frac{P_{mpp}(T_m, G_{POA})}{G_{POA}{\cdot}A_{m,act}} \tag{11}$$

where κ_P is the temperature coefficient of the P_{mpp} (%/K) obtained from [133].

3.4. Performance indicators

The use of the land equivalent ratio (LER) for assessing the performance of agrivoltaic systems was proposed in [5] and was defined as a sum of two ratios; AC electrical and crop yield of APV divided by the reference case:

$$LER = \frac{Y_{e,APV}}{Y_{e,ref}} + \frac{Y_{c,APV}}{Y_{c,ref}} \tag{12}$$

For crop yield the reference is an open field (FS conditions), while for

Table 5
List of annual efficiency terms associated with the conversion of solar energy into AC electrical yield.

Soiling [1]	PV module [2]	Module mismatch (MM)	Maximum power point tracker (MPPT)	Inverter [3]	Ohmic
98.3–100%	~16.9%	99.5% [128–129]	99% [130]	98.5% [131]	99% [132]

[1] Vary according to PV orientation; lowest for E-W hinged, highest for E-W vertical.
[2] Vary according to PV topology; lowest for E-W hinged, highest for E-W vertical.
[3] Estimated based on the weighted efficiency European model.

electrical yield it is a conventional GMPV array. To obtain a realistic LER the design of the latter should be optimized. As monofacial arrays can be employed in high PV densities, the design was tailored to maximize electricity production and land utilization (Table 6).

The formulation of a comprehensive crop yield model, which depends on various microclimatic parameters and crop genetic characteristics, is complex. Nonetheless, a reasonable estimate of crop yield reduction can be obtained based on the net CO_2 assimilation rate A [140]. For the study case of blueberries, this was achieved by simulating PAR incident on a horizontal plane at canopy height and relating that to A, through the trend provided in Fig. 1. The magnitude of light intercepted by each leaf will differ, depending on its orientation and location in the canopy. However, for this analysis, it was assumed that the crop is uniformly illuminated or shaded, which is partially justified by the diffuse cover and the frequently intermittent to overcast climate of Boston.

To estimate the seasonal variability of light, PAR at solar noon was obtained for two days per month: one with clear, and one with overcast sky conditions. Then, the corresponding net CO_2 uptake rates were determined for both open field conditions A_{FS}, and under shade A_{APV}:

$$\frac{Y_{c,APV}}{Y_{c,ref}} = \frac{c}{24}\left[\sum_{i=1}^{12}\left(\frac{A_{APV,i}}{A_{FS,i}}\bigg|_{cleardays} + \frac{A_{APV,i}}{A_{FS,i}}\bigg|_{overcastdays}\right)\right] \tag{13}$$

The parameter c signifies the loss of cultivatable land that is occupied by pillars, which lies between 2 and 10% depending on support structure and APV design [5,141]. For the case of blueberries, it was assumed that this loss is negligible ($c = 1$). In clear days, particularly during summer, the amount of PAR incident on crops largely surpasses the LSP. This is usually accompanied by high evapotranspiration rates that lead to stomata hydropassive closure; ultimately, reducing growth as shown in Fig. 1. Nonetheless, the positive effect of shading on crop productivity was neglected, since in open field conditions shading nets are usually applied. Thus, in FS conditions, when incident PAR was above the LSP, A_{FS} was set equal to the saturated growth rate (12 μmols/m^2/s). This might lead to an underestimation of crop yield. On the other hand, a significant portion of leaves within the canopy do not attain light saturation, due to partial shading.

Note that depending on the crop's phenological stage, the sensitivity of yield and quality to shading can vary. To simplify the analysis, it was assumed that each month contributed equally, irrespective of sky conditions, to the crop yield ratio. The latter is partially true, as blueberries can photosynthesize effectively even under overcast sky conditions. A weighted average could be used to account for important developmental stages of the crop. Finally, by considering PAR at solar noon only, diurnal changes that occur from the introduction of the APV array are omitted.

Because of the presence of the array, irradiance on ground is non-uniform, which can jeopardize the overall marketable yield of crops (depending on species and climatic conditions). The statistical measure used to assess light inhomogeneity was the coefficient of variation (CV), defined as the ratio of sample standard deviation σ to mean μ [142]:

$$CV = \frac{\sigma}{\mu} \tag{14}$$

4. Results & discussion

4.1. Array sensitivity – Macro scale

By omitting border effects, the influence of module elevation on ground irradiation diminished. The annual and average ground irradiation of the farm sample increased linearly by 3.4% when the array was raised from 2 to 7 m. Essentially, with higher elevation the sky view factor (SVF) of the ground increases, thus allowing additional diffuse horizontal irradiance (DHI) to penetrate. Nonetheless, BG was not affected considerably (data not shown). Therefore, the main incentive for elevating modules is to ensure that there is sufficient ground clearance (~4–5 m) for the operation of agricultural machinery [3]. Nonetheless, elevated modules benefit from free convection and the reduced dust deposition rate. Ultimately, to minimize capital costs and facilitate the operation of most machinery an elevation of 5 m was selected for the following simulations, apart from the study case of blueberries discussed in 4.3 Module sensitivity – micro scale.

To conceptualize how the deployment configuration of the array influences ground and POA irradiation – two main parameters used to assess the performance of APV – a multi-dimensional sensitivity analysis was performed. Generally, light availability on ground was significantly higher for E-W facing topologies; however, the gain with wider RS was lesser (Fig. 5 a and b). In specific, when the RS was doubled, ground irradiation increased from 58.1% to 79.6% for a south facing array with a 35° tilt, while for E-W facing and vertical it enhanced from 75.9% to 88.6%. In addition, for a wider RS, sensitivity to module orientation – tilt and azimuth – greatly diminished. This is reasonable as with decreasing PV density, the influence of orientation on ground irradiation decays.

The analysis is continued for the POA irradiation on both sides of the bifacial PV module (Fig. 5 c and d). Overall, S-N topologies received a higher amount of POA irradiation, which is mainly attributed to the low ground albedo. A wider RS amplified ground reflected irradiation subsequently increasing POA. This gain was depended on PV module orientation with the tilt angle being dominant. For example, when the RS of a south facing array was doubled it received a boost in POA by 3.1% (10° tilt), and 5.6% (50° tilt), while for E-W vertical the gain was 9%. Higher tilts become beneficial with increasing RS; consequently, promoting E-W vertical as a viable alternative. Ultimately, this will depend on ground albedo [66,76] and module bifaciality. Tilted modules further benefit since partial shading and masking between rows is mitigated. For topologies facing due south, the tilt that maximized POA was between 30 and 35°, depending on the RS. Nonetheless, optimum tilt was mainly dictated by absorption of the front side, similar to monofacial PV. For both topologies, POA irradiation sensitivity to orientation enhanced as the RS was widened. Nonetheless, the influence of the azimuth angle was not significant, and specifically for vertically installed it was negligible (less than 1% reduction in POA). Therefore, it is intriguing to orient arrays south-west, subsequently allowing increased light penetration for crops in the morning, while providing additional shading in the afternoon. In this way crop productivity is prioritized, without significantly affecting PV performance.

To conceptualize the underlying trade-offs of each APV topology, the RS was extended and its influence on agrivoltaic performance was investigated (Fig. 6). Both topologies followed a similar behaviour; as the RS was widened ground irradiation increased, while electrical yield decreased. Initially, the gain in ground irradiation was abrupt as overlapping ground shadows were resolved. Eventually, it saturated

Table 6
Key-parameters concerning the reference GMPV case occupying 2.7 ha of land.

Module elevation	Tilt angle	Azimuth angle [1]	Row spacing	Number of modules	AC electrical yield	Specific electrical yield
50 cm	18°	180°	270 cm	9900	3020 MWh/yr	1130 kWh/kWp

[1] Facing due south.

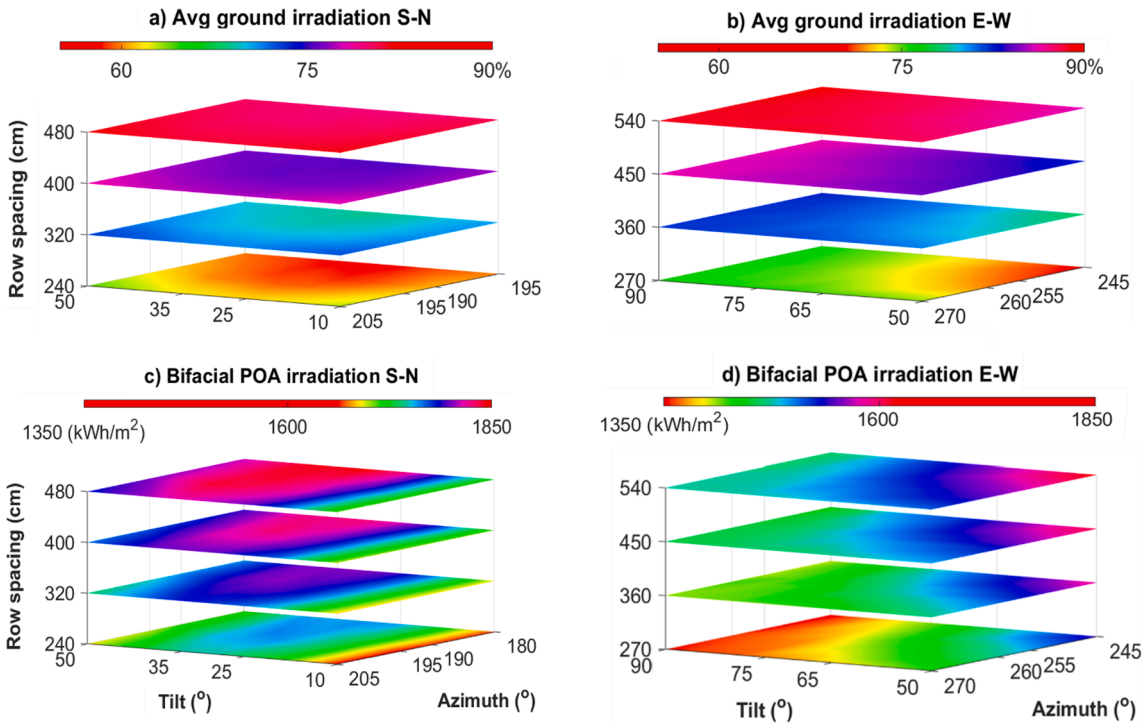

Fig. 5. Annual and average irradiation sensitivity to orientation and row spacing for two main topologies. Ground irradiation was expressed as percentage of full sun conditions, while for the plane of array (POA) irradiance a bifaciality of 90% was used.

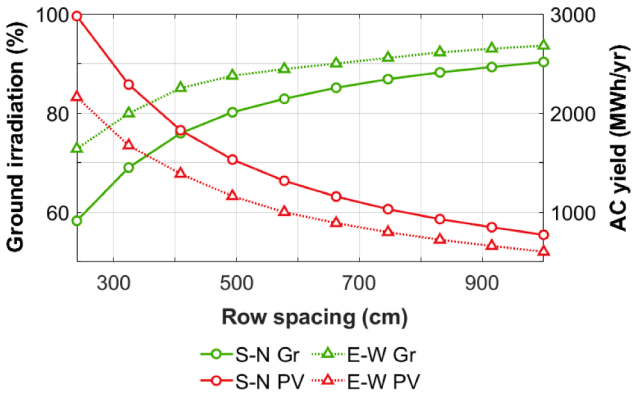

Fig. 6. Sensitivity of average ground irradiation and total AC yield (both annual) to PV topology and spacing. S-N facing topology: 33° tilt, 193° azimuth; while for E-W vertical: 90°, 260°. The energy yield of the reference GMPV is 3 GWh/yr.

following a logarithmic trend. Likewise, BG also saturated with increasing RS (data not shown). In reverse, energy yield portrayed a negative exponential trend. Essentially, a lower PV density decreases the overall energy yield of the APV farm, yet it maximizes light availability for both PV and crops. Hence, another trade-off arises; a sustainable or synergistic design, and one that exploits the land most effectively in terms of produced energy. However, the latter does not necessarily maximize LER since crop yield is greatly impinged depending on crop shade tolerance.

4.2. String sensitivity – Meso scale

Other string arrangements were investigated and compared to the conventional ones discussed previously. From those simulated four were selected (Fig. 7); S-N facing labelled as S1 and S2, and E-W vertical as E1 and E2 for conventional and checkerboard module arrangements, respectively. For S2 and E2 a wider RS was adopted to mitigate partial shading on modules and overlapping shadows on ground. Specifically, for topology E2, module elevation was decreased to 1.5 m, mainly due to the extended RS. Although machinery operating will not be allowed to pass under the array, farming activities can still proceed.

The agrivoltaic performance of each topology was assessed and compared to the conventional and separate production of food and energy (Fig. 8). Overall, annual AC yield was significantly impinged, due to the reduced PV density. Topologies S1 and S2 permitted a relatively higher electricity conversion mainly due to their orientation. In contrast, to facilitate crop growth in winter, E1 and E2 are non-optimal for direct light. This is also reflected on their specific yield (kWh/kWp), which is much lower than that of south facing; nonetheless, E-W vertical bifacial enabled a considerable gain (~13%) in comparison to optimally inclined monofacial PV. Furthermore, such PV configurations led to the lowest ground irradiation reduction. Overall, owing to the decreased PV density a reduction of the initial PV system cost is expected, which is proportionate to the total peak power installed [143].

To further investigate the unique features of each design the underlying shading pattern and schedule, ranging from hourly to monthly timescales, were examined. At first, daily ground irradiation and CV were simulated for one day per month, with May and December being displayed in Fig. 9. For clear days shading intensity and inhomogeneity increased significantly, unlike days with overcast or intermittent sky conditions. This was more apparent in winter, where solar elevation is lower, thus extending the length of shadows and the area of insufficient crop growth as depicted in purple. Nonetheless, due to the frequently intermittent climate of Boston, these inconsistencies averaged out on a larger timescale. This is verified by the cumulative ground irradiation and CV in Fig. 9 (c, f, i, l) for seasonal (mid-March to mid-Oct), and annual cultivation periods. E-W vertical topologies amplified light penetration, especially during the winter months; consequently, they are preferable for the cultivation of permanent crops that are grown throughout the year, while S-N facing are more suitable for summer. The conventional arrangements casted striped patterns; therefore, promoting intercropping and subsequently sustainable agriculture [144]. On

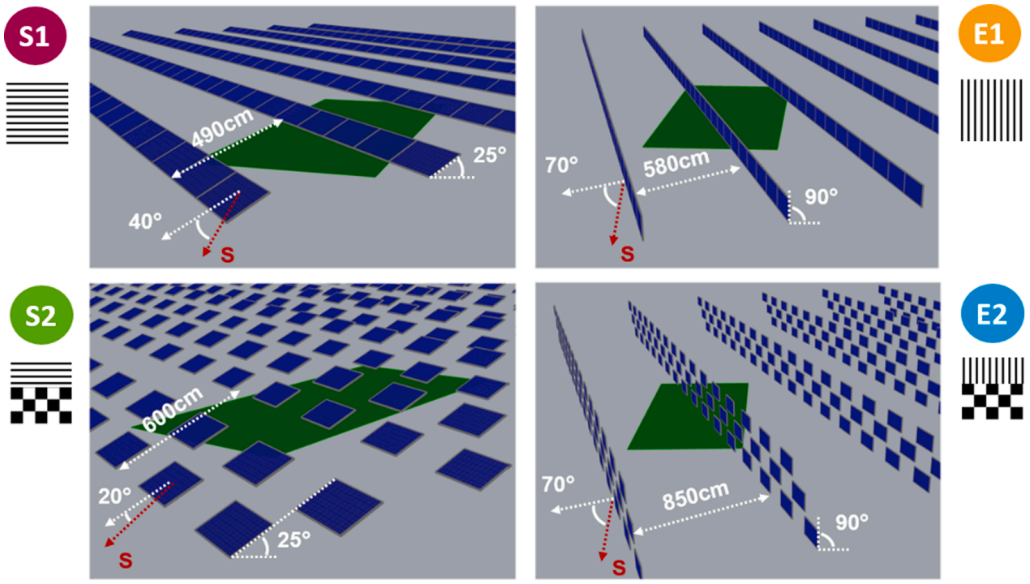

Fig. 7. Selected PV topologies: conventional module arrangement (S1, E1) and checkerboard (S2, E2).

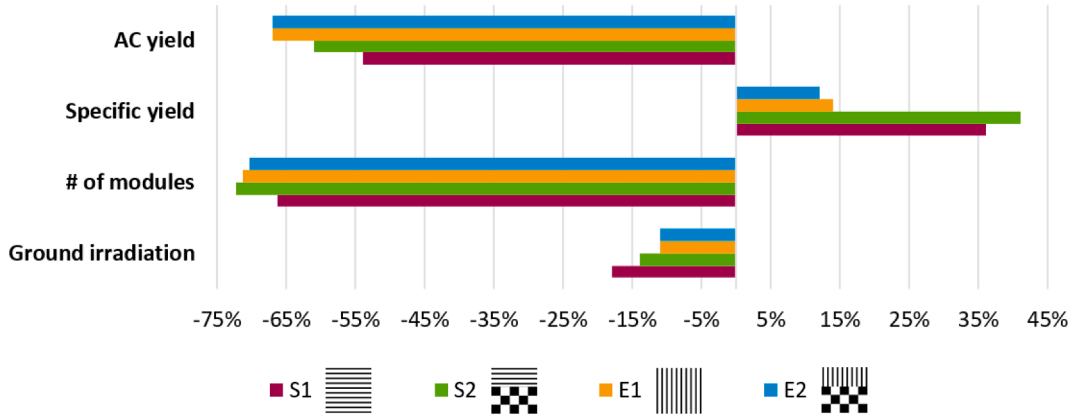

Fig. 8. Agrivoltaic performance of the selected topologies in comparison to the reference GMPV case. Note that ground irradiation reduction was related to full sun (open field) conditions.

the other hand, the checkerboard layout of topologies S2 and E2 resulted in a patchy shading layout with sharp irradiation gradients; thus, other arrangements should be investigated.

The evaluation of the shading schedule is continued for an hourly timescale (Fig. 10) for three distinct topologies. In south facing arrays the distribution of shade was non– homogeneous, it rather accumulated at a certain region. This effect was intensified during winter solstice. Contrary, E-W vertical topologies resulted in a more uniform distribution of shade. However, as they do not shade at noon, plant productivity is reduced due to the combination of high irradiance and temperature. To alleviate stomata mid-day hydropassive closure, the E-W wings topology is introduced, which offers semi-microclimatic control. Because of its orientation, crops are effectively shaded at noon, while light is distributed homogeneously throughout the day.

Based on these findings, when conventional modules are employed, S-N facing topologies should be used for shade tolerant crops and E-W wings those that necessitate shading at mid-day.

4.3. Module sensitivity – Micro scale

Through the previous analysis the limitations of conventional modules, due to their large size and opaqueness, were identified. These include non-homogeneous irradiance distribution (short timescales) and intense shading, thus necessitating reduced PV densities to maintain sufficient crop yields. By designing a customized module, tailored for the cultivation of a certain crop under a specific climate, it is possible to overcome these limitations. In particular, the micro-scale sensitivity was performed to investigate the cultivation of the 'bluecrop' highbush blueberry (*Vaccinium corymbosum*) under an E-W wings topology (Fig. 11 (a)). As it is a high value crop, the PV array was installed right above to offer protection against harmful weather conditions and irradiance during noon.

4.3.1. Glass extension

Various cell spacings and arrangements were examined; however, although light uniformity on ground was enhanced the gain in magnitude was not significant.

Therefore, other cover materials were examined such as the prismatic glass SG80 [50] with the given optical properties listed in Table 3. Through its integration, the overall fraction of diffuse light increased significantly, thus softening irradiation gradients, while amplifying ground albedo. As a result, soil evaporation is expected to be reduced. With increasing front cover length, PAR right below – on a horizontal plane and at canopy height – increased linearly (Fig. 11 (c)). At first glance, this effect might seem counter intuitive. However, since the translucent material was treated by Radiance as a Lambertian scatterer,

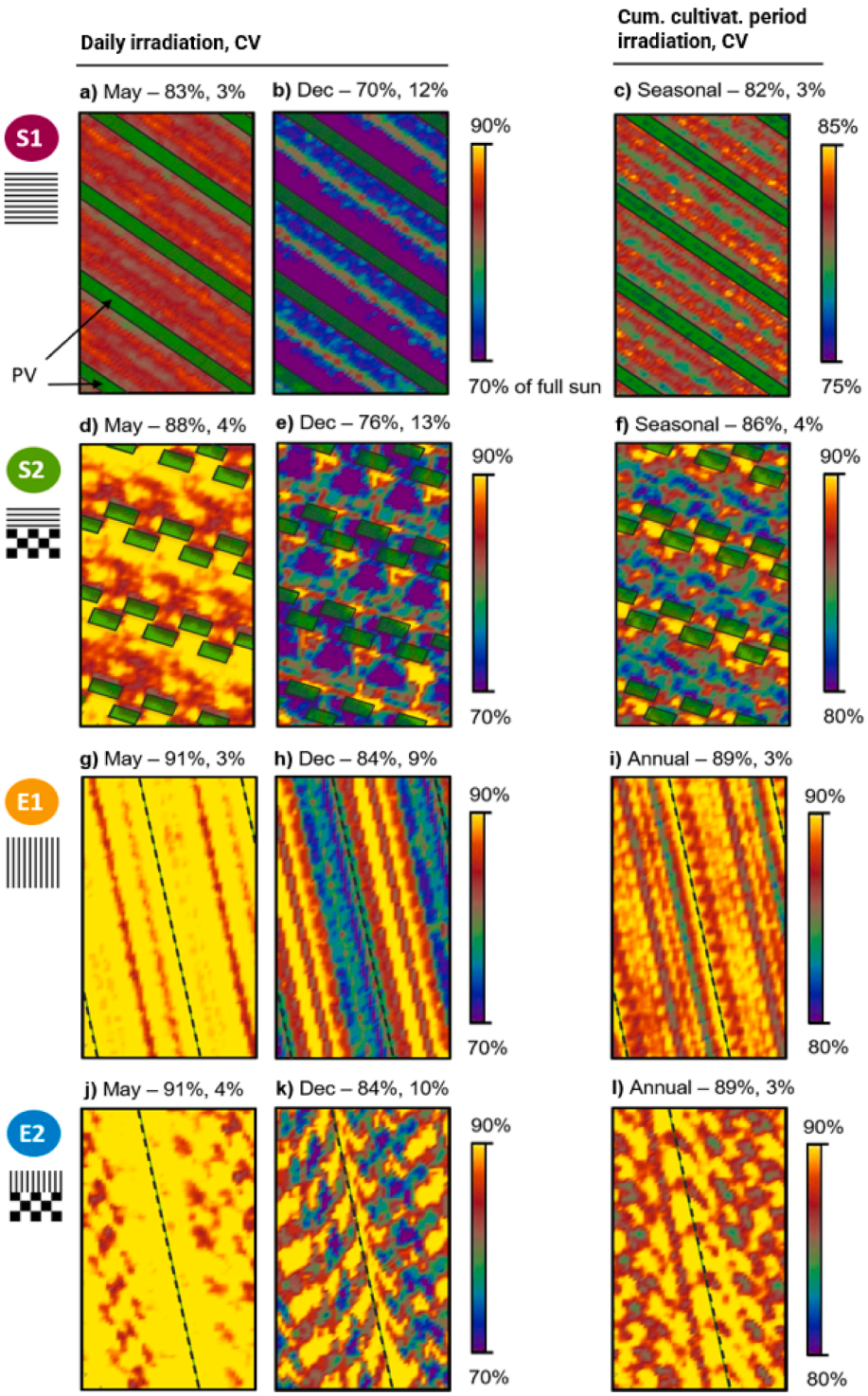

Fig. 9. Shading intensity and distribution on ground for the selected topologies. The average ground irradiation for each corresponding period and coefficient of variation (CV) are displayed. The daily irradiation is included for two days; one in May with intermittent to overcast sky conditions, and one in December with clear skies. Note that irradiation was calculated for a horizontal plane close to ground, which is applicable to low-height field crops.

the cover's scatter angle was not modelled appropriately. Hence, omitting saturation of transmitted irradiance on crops after a certain front cover extension. Through a trial-and-error process, the necessary extension of the top cover was determined to be 35 cm for each side.

4.3.2. Cell spacing & arrangement

By widening the spacing between cells, additional light is transmitted and converted into diffuse; ultimately, enhancing light interception by the crop. Yet another trade-off arises between energy yield and PAR at canopy height (Fig. 11 (d)). Analogous to the RS, the relationship between module transparency and irradiance was found to be logarithmic. A similar behaviour was observed for the BG, where an increase in transparency from 7% to 55% led to a boost in BG by 3.8%. Comparable results were found in [65]. In contrast, annual AC yield decreased with a linear slope. Note that the positive influence of decreased cell density on heat dissipation and module efficiency was not

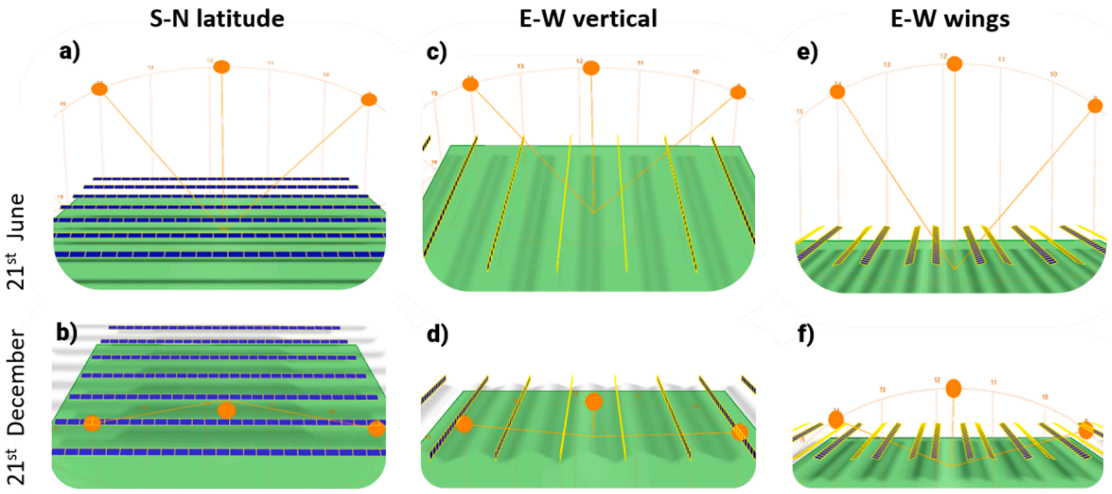

Fig. 10. Hourly shading distribution for three main PV topologies with shading patterns accumulated from three time-instants: morning, solar noon, and afternoon.

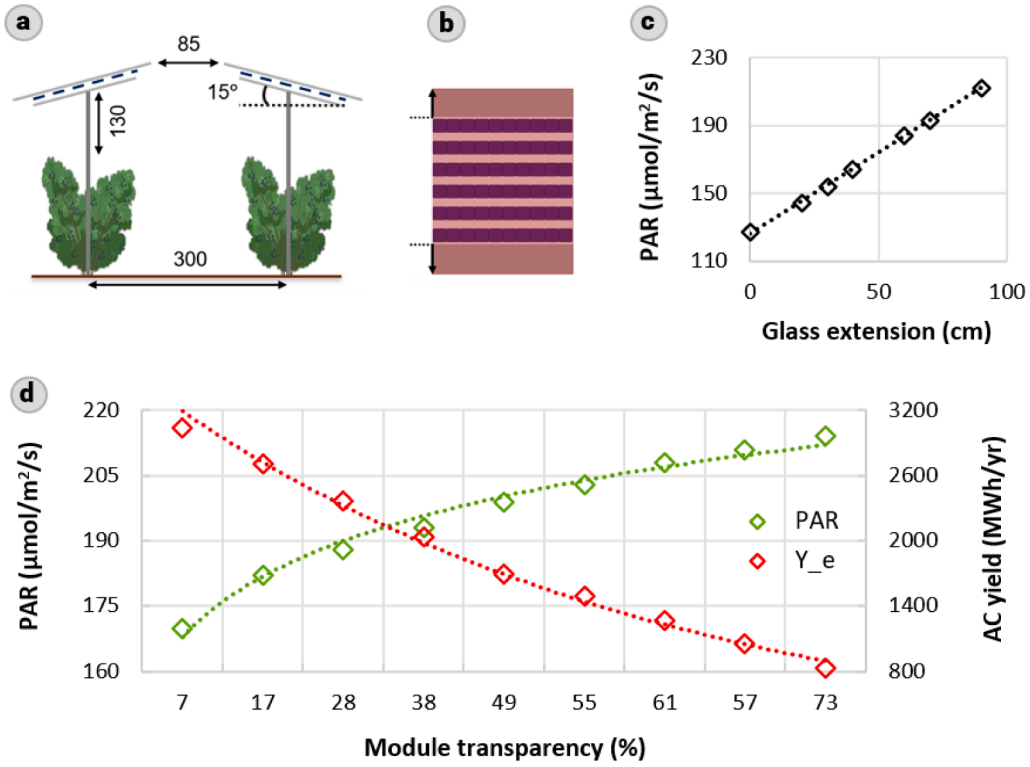

Fig. 11. (a) Front view of the E-W wings topology with dimensions given in cm. (b) Top cover extension with optimized cell layout. (c) PAR sensitivity to glass cover (SG80) extension. (d) PAR and annual AC yield sensitivity to cell spacing. PAR was simulated for a horizontal plane at canopy height, on the 21st of December (clear sky) at solar noon. The reference GMPV case produced 3 GWh/yr.

considered. To minimize yield reduction (~17%) of blueberries a module transparency of 38% was used. This value is unique for the E-W wings PV topology, and it refers to the fraction of inactive area within the module, while neglecting the area occupied by the extended front cover. Any additional increase of module transparency would lead to insufficient shading in summer, as well as heavily reduced AC yield.

4.3.3. Agrivoltaic performance

In general, crops are effectively shaded from harmful irradiance without impinging their growth. Simulation results of PAR (at canopy height) during solar noon can be observed in Fig. 12. Irradiance under shade is shown in blue, while the gain under FS conditions is displayed in orange. Irradiance reduction (shading rate) can vary from 20% in overcast up to 65% in clear sky conditions. This is desirable, since during clear days light saturation can occur, thus the shading rate is high. Even under an overcast sky the array permits sufficient light apart from some days in winter. Nevertheless, under such conditions, crops would not be able to attain saturation even in an open field.

Additional performance indicators were calculated (Table 7) for the E-W wings topology. Electrical yield was significantly enhanced (57% higher yield than topology S1). Furthermore, by utilizing a shade tolerant crop and a customised module, denser arrays can be installed. Although in relation to the reference GMPV array AC yield decreased, specific yield amplified owing to the integration of bifacial modules. The PV array's average BG was 15.4% (5–15% for conventional large-scale bifacial systems [62]). The simplified LER was found to be in the

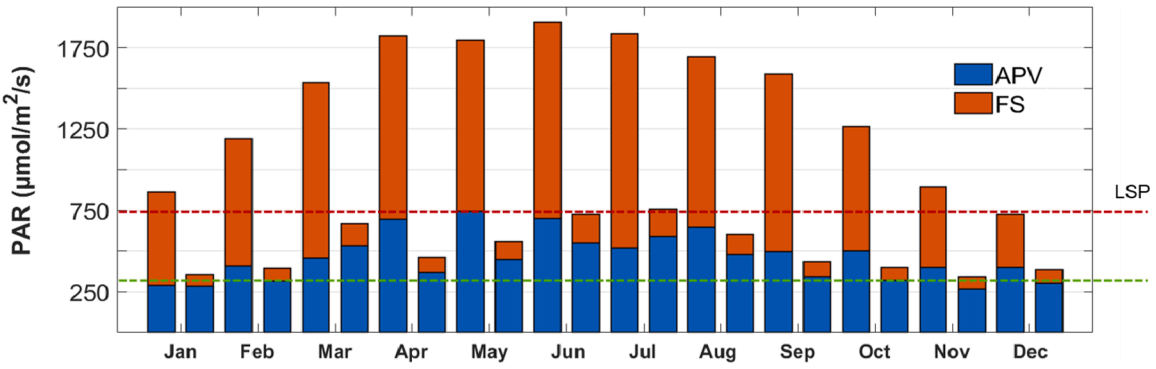

Fig. 12. PAR in full sun (FS) conditions and under shade (APV) during solar noon and throughout the year. Two days per month are shown, one with clear and the other with overcast sky conditions. The red line indicates the light saturation point of blueberries, while the green one sets the minimum light intensity necessary to attain at least 65% of the saturated growth rate.

Table 7
Performance of the E-W wings topology relative to the reference case (GMPV array and open field conditions).

AC yield	Specific yield	LER	# of modules	Inhomogeneity
−33%	18%	50%	−43%	2%

upper range of stationary APV systems [5,57,145] partly due to the moderate reductions in crop yield ratio. Note that the ground cover ratio (GCR) was determined to be 68%; however, by considering the increased cell spacing and glass transparency it was estimated to be 34.1%.

5. Conclusions

In this study, a series of insights were provided to promote the deployment of bifacial agrivoltaic arrays as they offer various synergistic effects with crop cultivation.

Irradiance homogeneity of PV module rear-side and bifacial gain (BG) were enhanced owing to the increased elevation, row spacing (RS), and customised module transparency. Specifically, as the row or cell spacing were widened, ground and subsequently PV rear-side irradiation amplified in a logarithmic fashion. Contrary, electrical yield reduced; however, this effect was partly mitigated by the augmented specific yield. In addition, deviation in module orientation – tilt and azimuth – from conventional topologies did not significantly diminish the potential of bifacial APV.

The performance and unique features of three main APV topologies were investigated. In comparison to a ground mounted monofacial PV array, specific yield increased by 39%, 18%, and 13% for S-N facing, E-W wings, and E-W vertical bifacial systems, respectively. South facing topologies are preferable for cultivation during summer and necessitate the use of shade tolerant species as they prioritize electricity generation. Contrary, E-W vertical enhanced the distribution and intensity of light, especially during winter; consequently, they are compatible with permanent crops. Finally, the E-W wings topology resulted in the most superior shading schedule and a partially controlled microclimate. Crop and APV topology selection are directly linked, therefore, it is crucial to know the appropriate shading rate and sequence before proceeding with the APV design.

To enhance the rate of photosynthesis under shade, modules were modified to have a wider cell spacing and a diffuse cover. For the cultivation of blueberries, through an E-W wings APV topology, land productivity increased by 50%, whereas energy yield reduced by 33% relative to the conventional and separate production of food and energy.

By conducting an individual assessment per selected bifacial APV array topology, their unique characteristics can be identified. When addressed properly, APV can provide supplementary functions; act as a shading element and offer protection against harmful weather conditions. These, along with the simultaneous and synergistic production of food and renewable energy establish this emerging PV sector as one of the main pillars of the energy transition.

CRediT authorship contribution statement

Odysseas Alexandros Katsikogiannis: Methodology, Software, Formal analysis, Investigation, Writing – original draft, Writing – review & editing, Visualization. **Hesan Ziar:** Conceptualization, Formal analysis, Writing – review & editing, Supervision. **Olindo Isabella:** Formal analysis, Supervision.

Declaration of Competing Interest

The authors declare that they have no known competing financial interests or personal relationships that could have appeared to influence the work reported in this paper.

References

[1] International Renewable Energy Agency IRENA. Renewable Power Generation Costs in 2019. Abu Dhabi, UAE; 2020. Retrieved from: https://www.irena.org/-/media/Files/IRENA/Agency/Publication/2020/Jun/IRENA_Power_Generation_Costs_2019.pdf.
[2] Capuano L. U.S. EIA International Energy Outlook 2020. Independent Statistics & Analysis; 2020. Retrieved from: https://www.eia.gov/outlooks/ieo/.
[3] Weselek A, Ehmann A, Zikeli S, Lewandowski I, Schindele S, Högy P. Agrophotovoltaic systems: applications, challenges, and opportunities. A review. Agron Sustain Dev 2019;39(4). https://doi.org/10.1007/s13593-019-0581-3.
[4] Goetzberger A, Zastrow A. On the coexistence of solar-energy conversion and plant cultivation. Int J Solar Energy 1982;1(1):55–69.
[5] Dupraz C, Marrou H, Talbot G, Dufour L, Nogier A, Ferard Y. Combining solar photovoltaic panels and food crops for optimising land use: towards new agrivoltaic schemes. Renew Energy 2011;36(10):2725–32. https://doi.org/10.1016/j.renene.2011.03.005.
[6] Sato D, Yamada N. Design and testing of highly transparent concentrator photovoltaic modules for efficient dual-land-use applications. Energy Sci Eng 2020;8(3):779–88. https://doi.org/10.1002/ese3.550.
[7] Yang F, Zhang Ye, Hao Y, Cui Y, Wang W, Ji T, et al. Visibly transparent organic photovoltaic with improved transparency and absorption based on tandem photonic crystal for greenhouse application. Appl Opt 2015;54(34):10232. https://doi.org/10.1364/AO.54.010232.
[8] Li Z, Yano A, Cossu M, Yoshioka H, Kita I, Ibaraki Y. Shading and electric performance of a prototype greenhouse blind system based on semi-transparent photovoltaic technology. J Agric Meteorol 2018;74(3):114–22. https://doi.org/10.2480/agrmet.d-17-00047.
[9] Domínguez C, Jost N, Askins S, Victoria M, Antón I. A review of the promises and challenges of micro-concentrator photovoltaics. AIP Conf Proc 2017;1881(1). https://doi.org/10.1063/1.5001441.
[10] Distler A, Brabec CJ, Egelhaaf H-J. Organic photovoltaic modules with new world record efficiencies. Progr Photovolt 2021;29(1):24–31. https://doi.org/10.1002/pip.3336.

[11] Yilmaz EC, Yesilyurt MK, Oner IV, Omeroglu G, Ozakin AN. Operational Stability and Degradation of Organic Solar Cells. Periodicals Eng Nat Sci (PEN) 2017;5:152–60. https://doi.org/10.21533/pen.v5i2.105.

[12] Croce R, van Amerongen H. Natural strategies for photosynthetic light harvesting. Nat Chem Biol 2014;10(7):492–501. https://doi.org/10.1038/nchembio.1555.

[13] Massa GD, Kim H-H, Wheeler RM, Mitchell CA. Plant productivity in response to LED lighting. HortScience 2008;43(7):1951–6.

[14] Marucci A, Cappuccini A. Dynamic photovoltaic greenhouse: Energy efficiency in clear sky conditions. Appl Energy 2016;170:362–76. https://doi.org/10.1016/j.apenergy.2016.02.138.

[15] Fischer M, Woodhouse M, Herritsch S, Trube J. International Technology Roadmap for Photovoltaic (ITRPV): 2019 Results. ITRPV – VDMA 2020;11:53–4.

[16] Department of Energy Resources, Department of Agricultural Resources. Guideline Regarding the Definition of Agricultural Solar Tariff Generation Units. MA, USA; 2018. Retrieved from: https://farmlandinfo.org/law/ma-smart-definition-of-agricultural-solar-tariff-generation-units/.

[17] Ziegler H. The evolution of stomata. Stanford, CA: Stanford University Press; 1987. p. 29–55.

[18] Li X, Chen W, Li Y. Study on photosynthetic characteristics of blueberry in greenhouse. Acta Hortic 2012;926:315–9. https://doi.org/10.17660/actahortic.2012.926.43.

[19] Tenhunen JD, Lange OL, Braun M, Meyer A, Losch R, Pereira JS. Midday stomatal closure in *Arbutus unedo* leaves in a natural macchia and under simulated habitat conditions in an environmental chamber. Oecologia 1980;47(3):365–7.

[20] Hopkins WG, Hüner Norman PA. Carbon assimilation and productivity. In: Introduction to Plant Physiology, 2nd ed. Hoboken: John Wiley & Sons; 2009: 257–62.

[21] Yin X, Struik PC. C3 and C4 photosynthesis models: An overview from the perspective of crop modelling. NJAS – Wageningen J Life Sci 2009;57(1):27–38. https://doi.org/10.1016/j.njas.2009.07.001.

[22] Boardman NK. Comparative photosynthesis of sun and shade plants. Annu Rev Plant Physio 1977;28(1):355–77.

[23] Bjorkman O, Boardman NK, Anderson JM, Thorne SW, Goodchild DJ, Pyliotis NA. Effect of light intensity during growth of Atriplex patula on the capacity of photosynthetic reactions, chloroplast components and structure. Yearbook Carnegie Instit Washington 1972;71:115–35.

[24] Bjorkman O, Holmgren P. Adaptability of the photosynthetic apparatus to light intensity in ecotypes from exposed and shaded habitats. Physiol Plant 1963;16:889–914.

[25] Bjorkman O, Holmgren P. Photosynthetic adaptation to light intensity in plants native to shaded and exposed habitats. Physiol Plant 1966;19:854–89.

[26] Burnside CA, Bohning RH. The effect of prolonged shading on the light saturation curves of apparent photosynthesis in sun plants. Plant Physiol 1967;32:61–3.

[27] Singh M, Ogren WL, Widholm JM. Photosynthetic characteristics of several C3 and C4 plant species grown under different light intensities. Crop Sci 1974;14:563–6.

[28] Woledge J. The effect of light intensity during growth on the subsequent rate of photosynthesis of leaves of tall fescue (Festuca arundinacea Schreb.) Ann Bot 1971; 35: 311–22.

[29] Jurik TW, Chabot JF, Chabot BF. Effects of light and nutrients on leaf size, CO2 exchange, and anatomy in wild strawberry (Fragaria virginiana). Plant Physiol 1982;70(4):1044–8.

[30] Wylie RB. Principles of foliar organization shown by sun–shade leaves from ten species of deciduous dicotyledonous trees. Am J Bot 1951;38(5):355–61.

[31] Crookston RK, Treharne KJ, Ludford P, Ozbun J. Response of beans to shading. Crop Sci 1975;15:412–6.

[32] Esau K. Plant Anatomy. New York: Wiley 1965; 2: 429–30.

[33] Nobel PS, Zaragoza LJ, Smith WK. Relation between mesophyll surface area, photosynthetic rate and illumination level during development of leaves of Plectranthus parviflorus Henckel. Plant Physiol 1975;55:1067–70.

[34] Turrell FM. The area of the internal exposed surface of dicotyledon leaves. Am J Bot 1936;23(4):255–64.

[35] Wylie RB. Principles of foliar organization shown by sun-shade leaves from ten species of deciduous dicotyledonous trees. Am J Bot 1951;38(5):355–61.

[36] Pearce RB, Lee DR. Photosynthetic and morphological adaptation of alfalfa leaves to light intensity at different stages of maturity. Crop Sci 1969;9:791–4.

[37] Atanasova L, Stefanov D, Yordanov I, Kornova K, Kavardzikov L. Comparative characteristics of growth and photosynthesis of sun and shade leaves from normal and pendulum walnut (Juglans regia L.) trees. Photosynthetica 2003;41(2). https://doi.org/10.1023/B:PHOT.0000011964.62378.5c.

[38] Mishra Y, Johansson Jänkänpää H, Kiss AZ, Funk C, Schröder WP, Jansson S. Arabidopsis plants grown in the field and climate chambers significantly differ in leaf morphology and photosystem components. BMC Plant Biol 2012;12(1). https://doi.org/10.1186/1471-2229-12-6.

[39] Sage RF, Mckown AD. Is C4 photosynthesis less phenotypically plastic than C3 photosynthesis? J Exp Bot 2005;57(2):303–17. https://doi.org/10.1093/jxb/erj040.

[40] Falster DS, Westoby M. Leaf size and angle vary widely across species: what consequences for light interception? New Phytol 2003;158:509–25. https://doi.org/10.1046/j.1469-8137.2003.00765.x.

[41] Tao L, Qichang Y. Advantage of diffuse light for horticultural production and perspectives for further research. Front Plant Sci 2015;6:3–4. https://doi.org/10.3389/fpls.2015.00704.

[42] Hovi T, Nakkila J, Tahvonen R. Interlighting improves production of year-round cucumber. Sci Hortic 2004;102(3):283–94. https://doi.org/10.1016/j.scienta.2004.04.003.

[43] Farquhar GD, Roderick ML. Pinatubo, diffuse light and the carbon cycle. Science 2003;299(5615):1997–8. https://doi.org/10.1126/science.1080681.

[44] Lakso AN, Musselman RC. Effects of Cloudiness on Interior Diffuse Light in Apple Trees. J Amer Soc Hort Sci 1976;101(6):642–4.

[45] Sheehy JE, Chapas LC. The Measurement and Distribution of Irradiance in Clear and Overcast Conditions in Four Temperature Forage Grass Canopies. J Appl Ecol 1976;13(3):831–40.

[46] Gu L, Baldocchi DD, Wofsy SC, Munger JW, Michalsky JJ, Urbanski SP, et al. Response of a Deciduous Forest to the Mount Pinatubo Eruption: Enhanced Photosythesis. Science 2003;299(5615):2035–8. https://doi.org/10.1126/science.1078366.

[47] Brodersen CR, Vogelmann TC, Williams WE, Gorton HL. A new paradigm in leaf-level photosynthesis: direct and diffuse lights are not equal. Plant, Cell Environ 2008;31:159–64. https://doi.org/10.1111/j.1365-3040.2007.01751.x.

[48] Markvart J, Rosenqvist E, Aaslyng JM, Ottosen CO. How is canopy photosynthesis and growth of Chrysanthemums affected by diffuse and direct light?. Retrieved from: Eur J Hort Sci 2010;75(6):253–8. https://www.researchgate.net/publication/289588578_How_is_Canopy_Photosynthesis_and_Growth_of_Chrysanthemums_Affected_by_Diffuse_and_Direct_Light.

[49] Hemming S, Mohammadkhani V, Dueck T. Diffuse Greenhouse Covering Materials - Material Technology, Measurements and Evaluation of Optical Properties. Acta Hortic 2008;797:469–75. https://doi.org/10.17660/actahortic.2008.797.68.

[50] Hemming, S. Light Transmission and Distribution in Vegetable Greenhouses. Presentation at the Canadian Greenhouse Conference, Niagara Falls, Canada; 2016. Retrieved from: https://www.canadiangreenhouseconference.com/attendee-information/speaker-program/speaker-program-wednesday/2016-presentations-for-posting/2016%20Light%20Transmission%20and%20Distribution_Hemming.pdf.

[51] Hemming S, van der Braak N, Dueck T, Elings A, Marissen N. Filtering natural light by the greenhouse covering – More production and better plant quality by diffuse light? Acta Hort 2005;711:105–10. https://doi.org/10.17660/ActaHortic.2006.711.10.

[52] Hemming S, Dueck T, Janse J, Noort FV. The effect of diffuse light on crops. Acta Hortic 2008;801:1293–300. https://doi.org/10.17660/actahortic.2008.801.158.

[53] Victoria NG, Kempkes F, Weel PV, Stanghellini C, Dueck T, Bruins M. Effect of A Diffuse Glass Greenhouse Cover on Rose Production and Quality. Acta Hortic 2012;952:241–8. https://doi.org/10.17660/actahortic.2012.952.29.

[54] Dueck T, Janse J, Li T, Kempkes F, Eveleens B. Influence of Diffuse Glass on the Growth and Production of Tomato. Acta Hortic 2012;956:75–82. https://doi.org/10.17660/actahortic.2012.956.6.

[55] Johnson DM, Smith WK. Low clouds and cloud immersion enhance photosynthesis in understory species of a southern Appalacian spruce-fir forest (USA). Amer J Bot 2006;93(11):1625–32. https://doi.org/10.3732/ajb.93.11.1625.

[56] Marrou H, Guilioni L, Dufour L, Dupraz C, Wery J. Microclimate under agrivoltaic systems: is crop growth rate affected in the partial shade of solar panels? Agric For Meteorol 2013;177:117–32. https://doi.org/10.1016/j.agrformet.2013.04.012.

[57] Amaducci S, Yin X, Colauzzi M. Agrivoltaic systems to optimise land use for electric energy production. Appl Energy 2018;220:545–61. https://doi.org/10.1016/j.apenergy.2018.03.081.

[58] Reher T, Willochx B, Cappelle J, Van de Poel B. Measurable Indicators of Agrivoltaic Crop Growth Potential. Poster presented at: AgriVoltaics 2020 – Launching Agrivoltaics World-wide; 2020 October 14-16; Online.

[59] Barron-Gafford GA, Pavao-Zuckerman MA, Minor RL, Sutter LF, Barnett-Moreno I, Blackett DT, et al. Agrivoltaics provide mutual benefits across the food–energy–water nexus in drylands. Nat Sustain 2019;2(9):848–55. https://doi.org/10.1038/s41893-019-0364-5.

[60] Marrou H, Wery J, Dufour L, Dupraz C. Productivity and radiation use efficiency of lettuces grown in the partial shade of photovoltaic panels. Eur J Agron 2013;44:54–66. https://doi.org/10.1016/j.eja.2012.08.003.

[61] Stein JS, Riley D, Lave M, Hansen C, Deline C, Toor F. Outdoor Field Performance from Bifacial Photovoltaic Modules and Systems. In: 2017 IEEE 44th Photovoltaic Specialist Conference (PVSC); 2017. https://doi.org/ 10.1109/PVSC.2017.8366042d.

[62] Reise C. "Realistic Yield Expectations for Bifacial PV Systems – an Assessment of Announced, Predicted and Observed Benefits". 6th PVPMC Workshop, Freiburg, Germany; 2016. Retrieved from http://www.slideshare.net/sandiaecis/42reiserealisticyieldexpectationsforbifacialpvsystems-56350717.

[63] Kreinin L, Bordin N, Karsenty A, Drori A, Gro*BG*eld D, Eisenberg N. PV module power gain due to bifacial design: preliminary experimental and simulation data. In: Proceedings of the 35th IEEE PVSC, Hawaii, USA; 2010:2171–5. DOI: 10.1109/PVSC.2010.5615874.

[64] Yusufoglu UA, Pletzer TM, Koduvelikulathu LJ, Comparotto C, Kopecek R, Kurz H. Analysis of the annual performance of bifacial modules and optimization methods. IEEE J Photovolt 2015;5(1):320–8. https://doi.org/10.1109/JPHOTOV.2014.2364406.

[65] Deline C, MacAlpine S, Marion B, Toor F, Asgharzadeh A, Stein JS. Assessment of Bifacial Photovoltaic Module Power Rating Methodologies - Inside and Out. IEEE J Photovolt 2017;7(2):575–80. https://doi.org/10.1109/JPHOTOV.2017.2650565.

[66] Sun X, Khan MR, Deline C, Alam MA. Optimization and performance of bifacial solar modules: A global perspective. Appl Energy 2018;212:1601–10. https://doi.org/10.1016/j.apenergy.2017.12.041.

[67] Yusufoglu UA, Lee TH, Pletzer TM, Halm A, Koduvelikulathu LJ, Comparotto C, et al. Simulation of Energy Production by Bifacial Modules with Revision of Ground Reflection. Energy Procedia 2014;55:389–95. https://doi.org/10.1016/j.egypro.2014.08.111.

[68] Asgharzadeh A, Marion B, Deline C, Hansen C, Stein JS, Toor F. A sensitivity study of the impact of installation parameters and system configuration on the performance of bifacial PV arrays. IEEE J Photovolt 2018;8(3):798–805. https://doi.org/10.1109/JPHOTOV.2018.2819676.

[69] Sugibuchi K, Ishikswa N, Obara S. Bifacial-PV power output gain in the field test using "EarthON" high bifaciality solar cells. In: 28th European Photovoltaic Solar Energy Conference. Paris, France; 2013. DOI: 10.4229/28thEUPVSEC2013-5BV.7.72.

[70] Huber A, Aberle AG, Hezel R. Temperature behavior of monofacial and bifacial silicon solar cells. In: 26th PVSC. Anaheim, CA, USA; 1997.

[71] Hezel R. Novel applications of bifacial solar cells. Prog Photovoltaics Res Appl 2003;11(8):549–56. https://doi.org/10.1002/pip.510.

[72] Faiman D, Dolev A. Optimum orientation of bi-facial PV modules. In: Proc. 19th Eur. Photovoltaics Sol. Energy Conf. Paris, France; 2004: 2470–3.

[73] Guerrero-Lemus R, Vega R, Kim T, Kimm A, Shephard LE. Bifacial solar photovoltaics - A technology review. Renew Sustain Energy Rev 2016;60:1533–49. https://doi.org/10.1016/j.rser.2016.03.041.

[74] Appelbaum J. Bifacial photovoltaic panels field. Ren Energy 2016;85:338–43. https://doi.org/10.1016/j.renene.2015.06.050.

[75] Shoukry I, Libal J, Kopecek R, Wefringhaus E, Werner J. Modelling of bifacial gain for stand-alone and in-field installed bifacial PV modules. Energy Procedia 2016;92:600–8. https://doi.org/10.1016/j.egypro.2016.07.025.

[76] Khan MR, Hanna A, Sun X, Alam MA. Vertical Bifacial Solar Farms: Physics, Design, and Global Optimization. Appl Phys 2017;206:240–8.

[77] Roy PS. Spectral reflectance characteristics of vegetation and their use in estimating productive potential. Proc Indian Acad Sci (Plant Sci) 1989;99(1):59–81.

[78] Gausman HW, Allen WA. Optical Parameters of Leaves of 30 Plant Species. Plant Physiol 1973;52(1):57–62.

[79] Gausman HW, Allen WA, Wiegand CL, Escobar DE, Rodriguez RR, Richardson AJ. Reflectance, transmittance, and absorptance of light of leaves for 11 plant genera with different leaf mesophyll arrangements. Texas A&M Univ. Tech. 1970; (7).

[80] Gausman HW, Allen WA, Schupp ML, Wiegand CL, Escobar DE, Rodriguez RR. The Leaf Mesophylls of Twenty Crops, their Light Spectra, and Optical and Geometrical Parameters; 1973.

[81] de Souza Filho CR. Introduction to Spectral Remote Sensing and Principles of Spectroscopy. [PowerPoint presentation]. Retrieved from: https://www.ige.unicamp.br/beto/GA235_2020/SR/Parte%201_Spectroscopy_Minerals_Vegetation_POS%202020.pdf.

[82] Gausman HW, Allen WA, Cardenas R. Reflectance of Cotton Leaves and Their Structure. Remote Sens Environ 1969;1(1):19–22.

[83] Jacobsen A, Broge NH, Hansen BU. Monitoring Wheat Fields and Grasslands Using Spectral Reflectance Data. International Symposium on Spectral Sensing Research (ISSSR), Melbourne, Victoria, Australia; 1995.

[84] Kuester T, Spengler D, Segl K, Guanter L, Kaufmann H. On the Spectral Resolution Requirements for the Derivation of Leaf Area Index from Hyperspectral Remote Sensing Data. EARSeL Workshop on Imaging Spectrospopy. Tel-Aviv, Israel; 2009. Retrieved from: https://www.researchgate.net/publication/228418616_On_the_Spectral_Resolution_Requirements_for_the_Derivation_of_Leaf_Area_Index_from_Hyperspectral_Remote_Sensing_Data.

[85] Nicolaï BM, Beullens K, Bobelyn E, Peirs A, Saeys W, Theron KI, et al. Nondestructive measurement of fruit and vegetable quality by means of NIR spectroscopy: A review. ScienceDirect 2007;46(2):99–118. https://doi.org/10.1016/j.postharvbio.2007.06.024.

[86] Adeh EH, Good SP, Calaf M, Higgins CW. Solar PV power potential is greatest over croplands. Sci Rep 2019;9(1). https://doi.org/10.1038/s41598-019-47803-3.

[87] Ziar H, Sönmez FF, Isabella O, Zeman M. A comprehensive albedo model for solar energy applications: Geometric spectral albedo. Appl Energy 2019;255:113867. https://doi.org/10.1016/j.apenergy.2019.113867.

[88] Zheng L, Zhao G, Dong J, Ge Q, Tao J, Zhang X, et al. Spatial, temporal, and spectral variations in albedo due to vegetation changes in China's grasslands. ISPRS J Photogramm Remote Sens 2019;152:1–12. https://doi.org/10.1016/j.isprsjprs.2019.03.020.

[89] Hirose T. Development of the Monsi–Saeki Theory on Canopy Structure and Function. Ann Botany 2005; 95: 493–4. https://doi.org/10.1093/aob/mci047.

[90] Monsi TM, Saeki T. Über den Lichtfaktor in den Pflanzengesellschaften und seine Bedeutung für die Stoffproduktion. Jap J Bot 1953;14:22–52.

[91] Saeki T. Interrelationships between leaf amount, light distribution and total photosynthesis in a plant community. Botanical Mag, Tokyo 1960;73(860):55–63.

[92] Blanke MM. Alternatives to reflective mulch cloth (Extenday) for apple under hail net? Sci Hortic 2008;116(2):223–6. https://doi.org/10.1016/j.scienta.2007.12.004.

[93] Overbeck V, Schmitz-Eiberger MA, Blanke MM. Reflective mulch enhances ripening and health compounds in apple fruit. J Sci Food Agric 2013;93(10):2575–9. https://doi.org/10.1002/jsfa.6079.

[94] Berrian D, Libal J. A comparison of ray tracing and view factor simulations of locally resolved rear irradiance with the experimental values. Prog Photovoltaics Res Appl 2020;28(6):609–20. https://doi.org/10.1002/pip.3261.

[95] Nussbaumer H, Janssen G, Berrian D, Wittmer B. Accuracy of simulated data for bifacial system with varying tilt angles and share of diffuse radiaton. Sol Energy 2020;197(6):6–21. https://doi.org/10.1016/j.solener.2019.12.071.

[96] Berrian D, Libal J, Klenk M, Nussbaumer H, Kopecek R. Performance of bifacial PV arrays with fixed tilt and horizontal single-axis tracking: comparison of simulated and measured data. IEEE J Photovolt 2019;9(6):1583–9. https://doi.org/10.1109/JPHOTOV.2019.2924394.

[97] Kang J, Reise C. Practical Comparison Between view factor method and ray-tracing method for bifacial PV system yield prediction. In: 36th European PV Solar Energy Conference and Exhibition. 2019. DOI: 10.4229/EUPVSEC20192019-5CV.3.30.

[98] Chiodetti M, Kang J, Reise C, Lindsay A. Predicting Yields of Bifacial PV Power Plants – What Accuracy Is Possible? EU PVSEC; 2018. https://doi.org/0.4229/35thEUPVSEC20182018-6CO.3.4.

[99] Chiodetti M, Lindsay A. Enhancing Bifacial Modelling with Ray-Tracing. PVPMC Workshop; 2016. DOI: 10.13140/RG.2.2.23758.00326.

[100] Hansen CW, Stein JS, Deline C, Macalpine S, Marion B, Asgharzadeh A, Toor F. Analysis of Irradiance Models for Bifacial PV Modules. In: 2016 IEEE 43rd Photovoltaic Specialists Conference (PVSC). 2016. https://doi.org/10.1109/pvsc.2016.7749564.

[101] Lo C, Lim Y, Rahman F. New integrated simulation tool for the optimum design of bifacial solar panel with reflectors on a specific site. Renew Energy 2015;81:293–307. https://doi.org/10.1016/j.renene.2015.03.047.

[102] Freeman J, Whitmore J, Nate B, Dobos AP. Validation of Multiple Tools for Flat Plate Photovoltaic Modelling Against Measured Data; 2014. Retrieved from: https://www.nrel.gov/docs/fy14osti/61497.pdf.

[103] Pelaez SA, Deline C. bifacial_radiance: a python package for modeling bifacial solar photovoltaic systems. J Open Source Software 2020; 5(50).

[104] Ward GJ. The Radiance lighting simulation and rendering system. In: Proceedings of the 21st annual conference on computer graphics and interactive techniques; 1994: 459–72.

[105] Kajiya JT. The rendering equation. Computr Graph 1986;20(4):143–50.

[106] Reinhart CF, Herkel S. The simulation of annual daylight illuminance distributions – A state of the art comparison of six RADIANCE-based methods. Energy Build 2000;32(2):167–87. https://doi.org/10.1016/S0378-7788(00)00042-6.

[107] Reinhart CF, Andersen M. Development and validation of a Radiance model for a translucent panel. Energy Build 2006;38(7):890–904. https://doi.org/10.1016/j.enbuild.2006.03.006.

[108] Reinhart CF, Walkenhorst O. Dynamic RADIANCE-based daylight simulations for a full-scale test office with outer Venetian blinds. Energy Build 2001;33(7):683–97. https://doi.org/10.1016/S0378-7788(01)00058-5.

[109] Perez R, Seals R, Michalsky J. All-weather model for sky luminance distribution – preliminary configuration and validation. Sol Energy 1993;50(3):235–45.

[110] Reinhart C, Breton PF. EXPERIMENTAL VALIDATION OF 3DS MAX® DESIGN 2009 AND DAYSIM 3.0. LEUKOS the J. of the Illuminating Eng. Society of North America. 2009. https://doi.org/10.1582/LEUKOS.2009.06.01001.

[111] Grasshopper [Computer software]. 2014. Retrieved from: https://www.grasshopper3d.com.

[112] Reinhart CF, Lagios K, Niemasz J, Jakubiec A. DIVA for Rhino Version 4.0. 2011. https://solemma.com/Diva.html/ [accessed on March 2020].

[113] Chudinzow D, Haas J, Díaz-Ferrán G, Moreno-Leiva S, Eltrop L. Simulating the energy yield of a bifacial photovoltaic power plant. Sol Energy 2019;183:812–22.

[114] Jung D, Gareis GH, Staiger A, Salmon A. Effects of Soiling on Agrivoltaic Systems: Results of a Case Study in Chile. Presented at: Agrivoltaics 2021; June. Online.

[115] Ravi S, Macknick J, Lobell D, Field C, Ganesan K, Jain R, et al. Colocation opportunities for large solar infrastructures and agriculture in drylands. Appl Energy 2016;165:383–92. https://doi.org/10.1016/j.apenergy.2015.12.078.

[116] Hottel H, Woertz B. Performance of flat-plate solar-heat collectors. Trans ASME 1942;64.

[117] Cano J, John JJ, Tatapudi S, Samy G, Mani T. Photovoltaic modules: Effect of tilt angle on soiling. Master's thesis. Arizona State Univ., Tempe, AZ, USA; 2011. Retrieved from: https://www.researchgate.net/publication/258543141_Photovoltaic_Modules_Effect_of_Tilt_Angle_on_Soiling.

[118] Bhaduri S, Kottantharayil A. Mitigation of soiling by vertical mounting of bifacial modules. IEEE J Photovolt 2019;9(1):240–4. https://doi.org/10.1109/jphotov.2018.2872555.

[119] Stoner ER, Baumgardner MF. Characteristic variations in reflectance of surface soils. Soil Sci Soc Am J 1981;45(6):1161–5. https://doi.org/10.2136/sssaj1981.03615995004500060031x.

[120] Baumgardner MF, Silva LRF, Biehl LL, Stoner ER. Reflectance properties of soils. Adv Agronomi 1986;38:1–44. https://doi.org/10.1016/S0065-2113(08)60672-0.

[121] Lillesand TM, Kiefer RW, Chipman JW. Remote sensing and image interpretation. Wiley 2004: 763. ISBN: 978-1-118-34328-9.

[122] Santbergen R, Zolingen RV. The absorption factor of crystalline silicon PV cells: A numerical and experimental study. Sol Energy Mater Sol Cells 2008;92(4):432–44. https://doi.org/10.1016/j.solmat.2007.10.005.

[123] Riverola A, Mellor A, Alonso Alvarez D, Ferre Llin L, Guarracino I, Markides CN, et al. Mid-infrared emissivity of crystalline silicon solar cells. Sol Energy Mater Sol Cells 2018;174:607–15. https://doi.org/10.1016/j.solmat.2017.10.002.

[124] Montero S, Pedro J, Nofuentes G, Diez JV. Spectral reflectance patterns of photovoltaic modules and their thermal effects. J Sol Energy Eng 2010;132. https://doi.org/10.1115/1.4002246.

[125] Taveres-Cachat E, Bøe K, Lobaccaro G, Goia F, Grynning S. Balancing competing parameters in search of optimal configurations for a fix louvre blade system with

integrated PV. Energy Procedia 2017;122:607–12. https://doi.org/10.1016/j.egypro.2017.07.357.
[126] SOLAR INNOVA. Reflectance of Solar Innova PV Modules. Retrieved from: http://www.importsunpv.com/marcas/solarinnova/Reflectance.of.Solar.Innova.PV.panels.pdf.
[127] Rubin M. Optical Properties of Soda Lime Silica Glasses. Solar Energy Mater 1985;12(4):275–88.
[128] Berrian D, Libal J, Peter C, Klenk M, Marco M, Nussbaumer H. Rear irradiance inhomogeneity of bifacial PV modules: Modelling and quantification by MoBiDiG. In: Presentation at the 6th Bifacail Workship, Amsterdam, NL; 2019.
[129] Deline C, Pelaez SA, MacAlpine S, Olalla C. Bifacial PV System Mismatch Loss Estimation and Parametrization. In: Presented at the 2019 European Photovoltaic Solar Energy Conference: Marseille, France; 2019. Retrieved from: https://www.nrel.gov/docs/fy20osti/73541.pdf.
[130] Smets A, Jäger K, Isabella O, van Swaaij R, Zeman M. Designing grid-connected PV-system. Solar Energy: The physics and engineering of photovoltaic conversion, technologies and systems. Cambridge, England: UIT Cambridge; 2016.
[131] M88H high efficiency three phase solar inverters for the European market - Data sheet. DELTA. 2017. https://krannich-solar.com/fileadmin/content/pdf/International/Delta_M88H.pdf.
[132] Almonacid F, Rus C, Pérez-Higueras P, Hontoria L. Calculation of the energy provided by a PV generator. Comparative study: conventional methods vs. artificial neural networks. Energy 2011;36(1):375–84. https://doi.org/10.1016/j.energy.2010.10.028.
[133] SolarWorld AG. Sunmodule Bisun SW 270 DUO Data sheet. 2016. https://www.solaricashop.com/download/solarworld/sw_bisun_270_en.pdf.
[134] King DL, Boyson WE, Kratochvill JA. Photovoltaic Array Performance Model; 2004. Doi: 10.2172/919131.
[135] D'Orazio M, Di Perna C, Di Giuseppe E. Experimental operating cell temperature assessment of BIPV with different installation configurations on roofs under Mediterranean climate. Renew Energy 2014;68:378–96. https://doi.org/10.1016/j.renene. 2014.02.009.
[136] Trinuruk P, Sorapipatana C, Chenvidhya D. Estimating operating cell temperature of BIPV modules in Thailand. Renew Energy 2009;34(11):2515–23. https://doi.org/10.1016/j.renene.2009.02.027.
[137] Zouine M, Akhassi M, Erraissi N, Aarich N, Bennouna A, Mustapha R, et al. Mathematical models calculating PV module temperature using weather data: experimental study. Lecture Notes Electr Eng 2018;519:630–9. https://doi.org/10.1007/978-981-13-1405-6_72.
[138] Barykina E, Hammer A. Modeling of photovoltaic module temperature using Faiman model: Sensitivity analysis for different climates. Sol Energy 2017;146:401–16. https://doi.org/10.1016/j.solener.2017.03.002.
[139] Lorenz E, Scheidsteger T, Hurka J, Heinemann D, Kurz C. Regional PV power prediction for improved grid integration. Prog Photovolt: Res Appl 2011;19:757. https://doi.org/10.1002/pip.1033.
[140] Zelitch I. The close relationship between net photosynthesis and crop yield. Am Instit Biol Sci 1982;32(10):796–802.
[141] Praderio S, Perego A. Photovoltaics and the agricultural landscape: the agrovoltaico concept. 2017. Retrieved from: http://www.remtec.energy/en/2017/08/28/photovoltaics-form-landscapes/.
[142] Kelley K. Sample size planning for the coefficient of variation from the accuracy in parameter estimation approach. Behav Res Methods 2007;39(4):755–66. https://doi.org/10.3758/BF03192966.
[143] Lindsay A, Chiodetti M, Dupeyrat P, Binesti D, Lutun E, Radouane K. Key elements in the design of bifacial PV power plants. In: 31st European Photovoltaic Solar Energy Conference and Exhibition; 2015: 1764–9. https://doi.org/10.4229/EUPVSEC20152015-5CO.14.4.
[144] Lithourgidis AS, Dordas CA, Damalas CA, Vlachostergios DN. Annual intercrops: an alternative pathway for sustainable agriculture. Aust J Crop Sci 2011; 5(4):396–410. ISSN: 1835-270.
[145] Riaz MH, Imran H, Younas R, Alam MA, Butt NZ. Module technology for agrivoltaics: vertical bifacial versus tilted monofacial farms. IEEE J Photov 2021;11(2):469–77. https://doi.org/10.1109/JPHOTOV.2020.3048225.